PHILOSOPHICAL TRANSACTIONS OF THE ROYAL SOCIETY A MATHEMATICAL, PHYSICAL & ENGINEERING SCIENCES

The Scope for Studies of Thin Surface Films on Metals and Alloys by Transmission Electron Microscopy of Ultramicrotomed Sections

K. Shimizu, K. Kobayashi, G. E. Thompson, G. C. Wood and P. Skeldon

Phil. Trans. R. Soc. Lond. A 1996 **354**, 213-235
doi: 10.1098/rsta.1996.0007

The scope for studies of thin surface films on metals and alloys by transmission electron microscopy of ultramicrotomed sections

By K. Shimizu[1], K. Kobayashi[1], G. E. Thompson[2], G. C. Wood[2] and P. Skeldon[2]

[1]*Department of Chemistry, Faculty of Science and Technology, Keio University, 3-14-1 Hiyoshi, Yokohama 223, Japan*

[2]*Corrosion and Protection Centre, University of Manchester Institute of Science and Technology, Manchester M60 1QD, UK*

Contents

Thin surface films on metals and alloys have immense practical significance in the protection and degradation of such materials under service conditions. The understanding of film morphology, composition and structure and their relation to the transport processes responsible for film growth, is essential in developing protection strategies. High resolution analytical transmission electron microscopy of sections of the films attached to the metal–alloy substrate provides a route towards the required understanding. Here, examples of various amorphous and crystalline films, together with films revealing amorphous to crystalline and crystalline to amorphous transformations during growth, are emphasized. Such situations illustrate the need for examination over a wide resolution range, defining with precision the general behaviour and specific local properties of crucial importance to corrosion science. Further, the direct observation approach is highly flexible, being applicable to both fundamental and practical situations with an easily understood technology transfer between them.

1. Introduction

Many features associated with the corrosion of metals and alloys involve migration of ionic species through thin surface films under a gradient of electrochemical potential. Such films may be oxides, corrosion products, or layers deliberately developed

Phil. Trans. R. Soc. Lond. A (1996) **354**, 213–235
Printed in Great Britain

or applied to provide a barrier between the corrosive environment and the metal substrate. Consequently, direct observation and analysis of the films, together with identification of the factors controlling their morphology, composition, structure and growth, are essential contributions to understanding and controlling the corrosion of metals and alloys generally. Observation and analysis of surface films on metals and alloys are generally not routine, because the films are usually thin (less than 1 μm), and may be morphologically, compositionally and structurally non-uniform. Additionally, such non-uniformity is related, in many cases, to microscopic heterogenities associated with the original metal surface of dimensions which can be resolved only by electron microscopy. Various surface analytical techniques, such as AES, XPS, SIMS, RBS, etc., are now available for compositional analysis of thin surface films on metals and alloys; additionally synchrotron approaches and mas-NMR provide structural probes. However, such techniques lack resolution in several dimensions. In cases where the films are microscopically non-uniform, interpretation of the data is thus limited by potential confusion resulting from signal averaging over the relatively large sampling area analysed. For detailed information on the morphology, structure and composition of thin, microscopically non-uniform films on metals and alloys with a high degree of depth and lateral resolution, cross-sectional transmission electron microscopy of the films attached to their metal substrates is essential. Thus the preparation of the sections of the surface films and their substrates, suitably thin for transmission electron microscopy, is a challenge which must be met for the successful understanding of the growth of the various surface films on metals and alloys and to gain insight into their role in the corrosion and protection of metals and alloys.

In addition to ion beam thinning, the ultramicrotomy approach, which has been advanced at the UMIST Corrosion and Protection Centre for many years, provides a successful method for the preparation of cross-sectional specimens of metals and their surface films as thin as 10 nm or less, with negligible damage to the film material (Thompson *et al.* 1991). This, allied with advances in sophistication of modern transmission electron microscopy, then enables real film material attached to its metal substrate to be examined at atomic-scale resolution, with simultaneous analysis (both compositional and structural) of local areas down to a few nanometres in diameter, yielding important information which cannot be readily obtained by other surface analytical techniques. Here, selected examples are presented and reviewed briefly to show the scope and flexibility of the approach, and the precise detail of the nature of various surface films on metals and alloys gained by direct observation and allied analysis.

2. Barrier oxide films on aluminium and tantalum

Fundamental aspects of the anodic oxide growth processes on aluminium and tantalum at ambient temperatures have been studied widely (Young 1961; Dignam 1972). The relevant anodic oxides are normally amorphous and highly uniform in thickness. Thus definition and understanding of epitaxial interactions between the metal and oxide, usually resulting in the development of a so-called mosaic structure of the oxide, with extensive arrays of potential paths for easy diffusion, are neither possible nor necessary. However, the ionic transport processes involved in the anodic oxide growth are considerably more complex than had been thought in the earlier

PHILOSOPHICAL TRANSACTIONS OF THE ROYAL SOCIETY A MATHEMATICAL, PHYSICAL & ENGINEERING SCIENCES

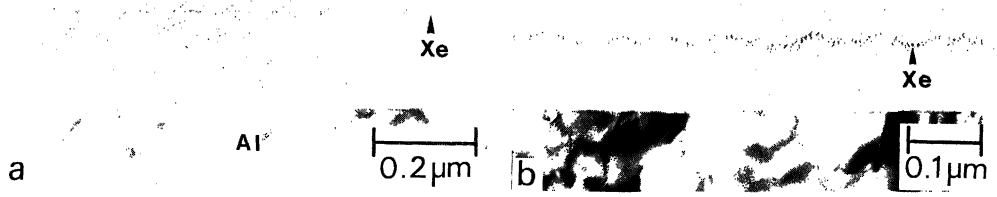

Figure 1. Xenon marker layers in barrier oxide films formed on aluminium in different electrolytes, after a thin pre-formed layer was implanted with xenon marker. (*a*) Film formed at a constant current density of 2 mA cm^{-2} in 5 wt% ammonium pentaborate solution to 300 V at 23 °C. (*b*) Film formed at a constant current density of 10 mA cm^{-2} in a borate-glycol electrolyte to 180 V at 25 °C.

models of ionic conduction, involving field-assisted, hopping transport of Frenkel defects (Young 1961; Verwey 1935). In the amorphous alumina structure, in the presence of a field in the 10^6–10^7 V cm^{-1} range, both metal and oxygen ions are mobile to approximately comparable extents, in an highly correlated manner, with new oxide growth occurring simultaneously at the oxide–electrolyte and metal–oxide interfaces respectively (Davies *et al.* 1965; Pringle 1973*a*, *b*). Since the oxide growth at the oxide–electrolyte interface is accompanied by the incorporation of anion species from the electrolyte, the barrier oxide films on aluminium and tantalum consists of two distinct layers: an outer layer doped with the anion species of the electrolyte and an inner layer of pure oxide (Randall *et al.* 1965; Dell'Oca 1970).

For compositional analysis of such thin, amorphous oxide films of uniform thickness and electrolyte anion uptake, grown over relatively smooth metal surfaces, various modern surface analytical techniques can be used routinely. Nevertheless, direct observation and analysis of the real film material in section, at high resolution, has several unique and important advantages over the indirect techniques, which are now considered.

For situations where oxide formation involves migration of both metal and oxygen ions, determination of transport numbers of the respective species crucial for detailed understanding of the ionic migration processes involved in the oxide growth. The transport numbers of metal and oxygen during anodic oxide growth are usually determined using noble gas markers (Davies *et al.* 1965; Pringle 1973*a*). In these experiments, a thin pre-formed oxide layer is initially labelled with the ion-implanted noble gas markers, such as xenon and radon; subsequently the oxide film is thickened by further anodizing. The position of the noble gas markers in the final oxide can then be determined by various techniques, including β- or α-ray spectroscopy (Davies *et al.* 1965), chemical sectioning combined with β-ray spectroscopy (Pringle 1973*b*), or by RBS (Brown & Mackintosh 1973). Importantly, however, cross-sectional transmission electron microscopy of the oxide films allows direct observation of the xenon marker layer and its location for the precise determination of transport numbers (Shimizu *et al.* 1981*c*).

Figure 1*a* shows a transmission electron micrograph of an ultramicrotomed section of a barrier oxide film, formed on aluminium in an aqueous borate solution after a thin pre-formed oxide was implanted with a xenon marker. The xenon marker is observed clearly within the oxide layer as a dark line running parallel to the flat oxide–

electrolyte and metal–oxide interfaces. From the micrograph, the marker position can be determined directly and precisely within an error of around 1 nm, giving a value of 0.44 for the transport number of metal. Such high precision cannot be readily achieved in the determination of the marker position by β- or α-ray spectroscopy or by RBS, where the energy loss parameters for β-ray or α-particles within amorphous alumina are not known with high precision.

For the barrier oxide growth on aluminium in an aqueous borate solution, it is clear that the transport numbers of the metal and oxygen are highly uniform across the film section, evident from the straight marker layer running parallel to the flat metal–oxide and oxide–electrolyte interfaces. However, this is not always the case. Complex behaviour is observed for the oxide grown in a phosphate solution or in a borate-glycol electrolyte. Here, the xenon marker layer does not run parallel to the flat oxide–electrolyte and metal–oxide interfaces, but exhibits an irregular undulation, as shown in figure 1*b*. From the micrograph, it appears that the transport number of the metal fluctuates in the range 0.44–0.54. Evidence accumulated so far suggests that such variations are genuine and are not only due to the presence of the xenon marker. Although further investigations are needed to clarify the nature of the as yet unidentified preferred paths, it is evident that such local and microscopical variations in the transport numbers can only be detected readily by cross-sectional transmission electron microscopy of the oxide films. Otherwise, the local, microscopic and irregular variations in the marker position could lead to the erroneous interpretation that general broadening of the marker layer occurs during the growth of the oxide in a phosphate or borate-glycol electrolyte.

The duplex structure of the barrier oxide films on aluminium and tantalum is also observed directly by transmission electron microscopy of ultramicrotomed sections of the respective films (Shimizu *et al.* 1981*b*). Transmission electron micrographs of ultramicrotomed sections of the barrier oxide films formed on aluminium in ammonium pentaborate, sodium tungstate and sodium molybdate solutions are shown in figures 2*a*–*c*, respectively. Differences are immediately evident among these films. Thus for the films formed in the electrolytes containing oxy-anions of heavy metals with greater scattering cross-sections for the electron beam, such as WO_4^{2-} and MoO_4^{2-}, the outer layer doped with the respective electrolyte anion species is readily distinguished from the inner pure oxide layer by its darker appearance, due to atomic number contrast effects (figures 2*b*, *c*). Also, it is evident that the proportion of the outer, anion-doped layer to the total film thickness, $d_{\mathrm{out}}/d_{\mathrm{total}}$, is different for the films formed in sodium tungstate and sodium molybdate solutions respectively, even though the oxide film growth in these electrolytes proceeds at nearly 100% current efficiency under the conditions used here. From the micrographs, $d_{\mathrm{out}}/d_{\mathrm{total}}$ is estimated to be 0.29 and 0.19 for the films formed in sodium tungstate and sodium molybdate solutions respectively. The different extents of the respective electrolyte anion-doped layers arises from a field induced transformation of the originally incorporated anion to an outwardly mobile catonic species.

For the barrier oxide films formed on tantalum, on the other hand, the duplex structure is observed only for films grown in phosphate solutions where significant anion incorporation occurs. In this case, the outer layer, doped with phosphate species with a reduced electron scattering cross-section, is readily differentiated from the inner pure oxide layer by its 'lighter' appearance (Shimizu *et al.* 1989).

Unlike the films formed in sodium tungstate or sodium molybdate solution, the films formed on aluminium in borate, phosphate, tartrate, citrate solutions or in a

PHILOSOPHICAL TRANSACTIONS OF THE ROYAL SOCIETY A MATHEMATICAL, PHYSICAL & ENGINEERING SCIENCES

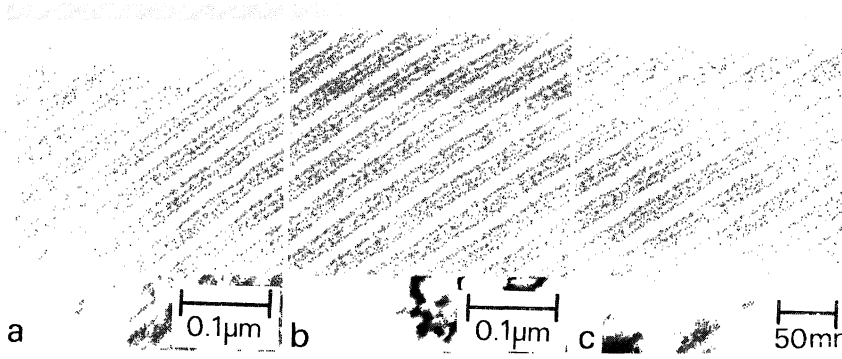

Figure 2. Transmission electron micrographs of ultramicrotomed sections of barrier oxide films formed on aluminium in different electrolytes. The films were formed at a constant current density of 5 mA cm^{-2} in 0.1 M solutions of the respective electrolytes at 25 °C. (*a*) Film formed at 300 V in an ammonium pentaborate solution. (*b*) Film formed to 250 V in a sodium tungstate solution. (*c*) Film formed to 175 V in a sodium molybdate solution.

borate-glycol electrolyte appear initially uniform in contrast in the transmission electron microscope. No layered appearance is immediately evident (figure 2*a*). However, even for such films, the outer, anion-doped layer and the inner pure oxide layer can be differentiated readily by transmission electron microscopy of ultramicrotomed sections simply by extending observations in the microscope over a period of 10 min to encourage crystallization of the originally amorphous alumina to γ-alumina (Shimizu *et al.* 1981*a*). Here, a key feature is that electron-beam-induced crystallization proceeds more readily in the inner pure oxide layer than the outer layer doped with the respective anion species, with the development of a sharp demarcation line separating the layers of differing susceptibilities to crystallization. Thus figure 3 reveals a section similar to figure 1*a*, but after it had been exposed to a defocused electron beam for about 10 min. As a result of electron irradiation, the inner pure oxide layer below the xenon marker layer appears to have been completely crystallized. Conversely, the outer layer above the marker layer, doped with borate species, still remains largely amorphous. However, the amorphous–crystalline boundary, indicated by a white line, appears to be located slightly above the xenon marker layer. This is due to the relatively slow growth of crystalline γ-alumina, which had nucleated in the inner pure oxide layer at locations close to the boundary between the outer and inner layer, into the outer layer doped with borate species. Consequently, the position of the amorphous–crystalline boundary appears slightly above its true location. If this is taken into consideration, the location of the boundary separating the outer, borate-doped layer and the inner pure oxide layer coincides with that of the xenon marker layer, indicating that the borate species incorporated into the thickening oxide are immobile during film growth.

Comparison between the xenon marker position and the location of the boundary separating the outer, anion-doped layer and inner pure oxide layer, however, indicates that the behaviour of electrolyte anions incorporated into the oxide, or species derived from the incorporated electrolyte anions, is considerably more complex than thought previously (Skeldon *et al.* 1985; Thompson *et al.* 1987). For the films formed on aluminium in sodium tungstate and sodium molybdate solutions, the boundary separating the outer, anion-doped layer and the inner pure oxide layer is located well above the xenon marker layer, or close to the oxide–electrolyte interface (fig-

Figure 3 Figure 4

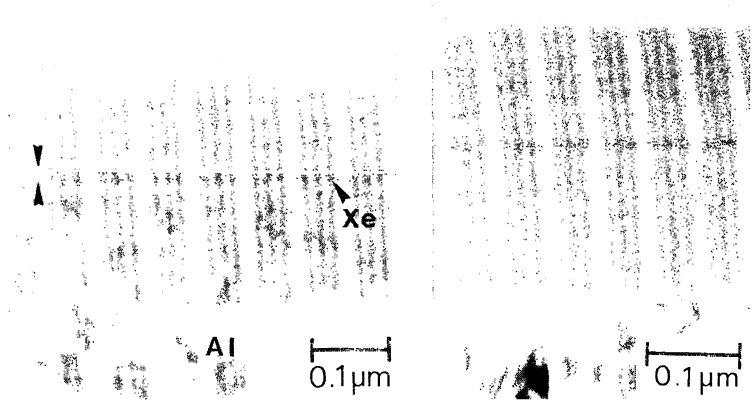

Figure 3. As figure 1*a*, but after 10 min exposure in the defocused electron beam of the transmission electron microscope to encourage crystallization.
Figure 4. Transmission electron micrograph of an ultramicrotomed section of a barrier oxide film formed on aluminium at a constant current density of 5 mA cm^{-2} in 0.1 M sodium tungstate solution to 250 V at 25 °C, after a thin pre-formed oxide layer was implanted with a xenon marker layer.

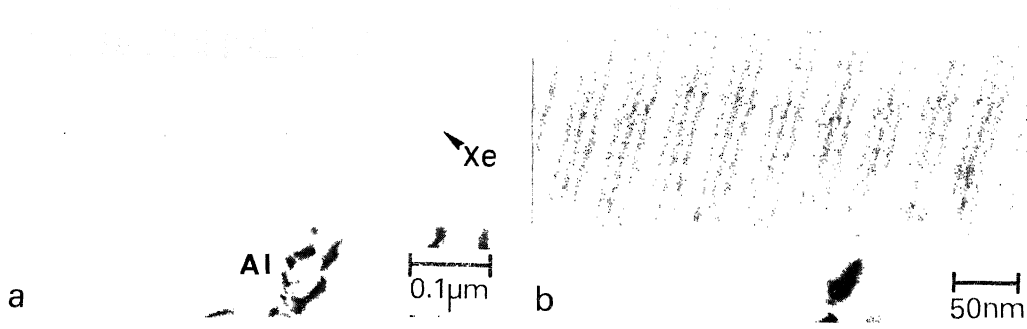

Figure 5. (*a*) Transmission electron micrograph of ultramicrotomed section of the barrier oxide film formed on aluminium at a constant current density of 5 mA cm^{-2} in 0.1 M ammonium dihydrogen phosphate solution to 180 V at 25 °C, after a thin preformed oxide layer was implanted with a xenon marker layer. (*b*) As (*a*), but after 10 min exposure with a defocused electron beam to encourage crystallization.

ure 4). Direct interpretation suggests that the W^{6+} and Mo^{6+} ions derived from the incorporated tungstate and molybdate species migrate outwards towards the oxide–electrolyte interface at rates less than that of Al^{3+} ions. Conversely, for the films formed in phosphate, tartrate, citrate and borate-glycol solutions, the boundary separating the outer anion-doped layer and the inner pure oxide layer is located well below the xenon marker layer, or close to the metal–oxide interface, as shown in figure 5. It also appears that the boundary separating the outer, phosphate-doped layer exhibits an irregular undulation which follows closely that of the xenon marker layer. Again, direct interpretation indicates that negatively charged anion species, such as PO_4^{3-} and carboxylate ions, migrate inwards or towards the metal–oxide interface at rates slower than that of oxygen ions (Skeldon *et al.* 1994).

In addition to the comparable migrations of metal and oxygen ions and the com-

PHILOSOPHICAL TRANSACTIONS OF THE ROYAL SOCIETY A MATHEMATICAL, PHYSICAL & ENGINEERING SCIENCES

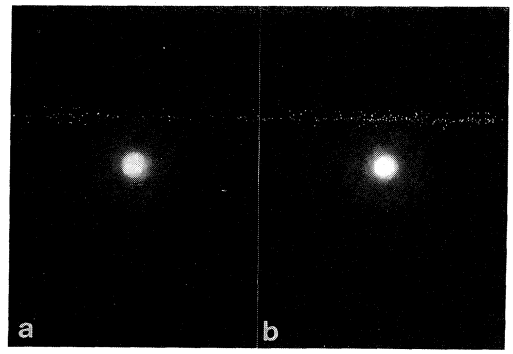

Figure 6. Microdiffraction patterns obtained from the inner, pure oxide layer of anodic alumina. (*a*) Before annealing. (*b*) After annealing at 450 °C for 1 h.

plex behaviour of the electrolyte anions incorporated into the oxide, a further key characteristic associated with the ionic migrations involved in the growth of anodic oxide films on aluminium and tantalum is that the ionic conductivity of the oxide films decreases markedly if annealing is carried out after anodizing (Vermilyea 1957; Young 1960; Crevecoeur & de Wit 1960). This has been interpreted in terms of 'structural ordering' of the amorphous oxide (Vermilyea 1957). Since, however, the annealing temperature is usually in the range between 100 and 450 °C, the oxides remain amorphous when probed by X-ray and conventional electron diffraction. Thus the nature of 'structural ordering' has remained unspecified until recently, despite its importance in the understanding of ionic migrations involved in oxide growth generally.

Microdiffraction is an extremely powerful technique for studying subtle structural differences in 'X-ray amorphous' materials (Brown 1988). With modern transmission electron microscopes, a very fine electron beam, of a diameter less than 10 nm and a convergent beam angle as low as 2×10^{-3} rad, is readily available for diffraction analysis. Thus the preparation of extremely thin ultramicrotomed sections, less than 10 nm thick, enables diffraction patterns to be extracted from exceedingly small volumes, about 1000 nm^3, of the real film material. Diffraction patterns extracted from such fine volumes reveal structural information in the 'X-ray amorphous' oxide films on aluminium and tantalum (Shimizu *et al.* 1990*a*, 1991*c*). An additional advantage of ultramicrotomed sections is that separate probing of the outer, anion-doped layer and the inner pure oxide layer is possible.

Microdiffraction patterns obtained from the inner pure oxide layer of anodic alumina are shown in figure 6. Before annealing at elevated temperatures, only diffuse haloes, corresponding to values of $(\sin Q)/\lambda$ of 0.16 and 0.37 $Å^{-1}$, are observed (figure 6*a*). Such diffuse haloes were considered to arise from scattering from units of the amorphous structure which is based on γ-Al_2O_3 (Kerr 1956). High resolution images of ultramicrotomed sections of aluminium supporting alumina films also confirm the amorphous nature of the original oxide, with the short range order unit appearing as a speckled background (Timsit *et al.* 1984), with crystalline material developing after electron beam irradiation (Timsit *et al.* 1985). However, after deliberate, annealing at 450 °C, a temperature considerably lower than that necessary to initiate the amorphous to γ-alumina transformation, 'crystalline speckles' are observed clearly within the diffuse haloes (figure 6*b*), indicating the development of a relatively low volume

fraction of microcrystalline regions in the amorphous oxide (Shimizu *et al.* 1990*a*). The reduction in the ionic conductivity in the annealed oxide is due to the presence of such microcrystalline regions which hinder the usual ionic transport processes in the amorphous oxide. However, upon reapplication of a high field, Al^{3+} and O^{2-} ions are injected from the surface of the microcrystalline regions into the surrounding amorphous regions. Consequently, the effective diameters of the microcrystalline regions fall below the critical size for a stable presence and the ionic conductivity of the oxide increases, eventually regaining its original value.

Microdiffraction analysis of the ultramicrotomed sections of the barrier oxide on tantalum also revealed striking features. Microcrystalline regions are present in the oxide without the need for annealing at elevated temperatures. Additionally, microcrystallinity of the oxide appears to be greater in the inner pure oxide layer than the outer layer doped with phosphate species (Shimizu *et al.* 1991*c*). Structural information of this kind is essential in the eventual development of integrated mechanisms of ionic transport through the amorphous oxide structure in the presence of a high electric field.

3. Anodic oxide films on aluminium containing crystalline material

Barrier oxide films on aluminium are normally amorphous, as described previously. However, the growth of crystalline barrier oxide is observed on aluminium surfaces which are initially covered with thin layers of thermal oxide or hydrous oxide which themselves contain some crystalline material (Kobayashi & Shimizu 1986). These crystalline barrier oxide films are of great practical importance as dielectric layers of aluminium electrolytic capacitors, since they can sustain higher voltages than the corresponding amorphous oxide films. However, their structures and mechanisms of growth are considerably more complex than the usual amorphous oxide material. The enormous potential of cross-sectional transmission electron microscopy is realized fully in the structural examination of the crystalline barrier oxide films. Indeed, the following description reveals that it is only after the application of transmission electron microscopy of ultramicrotomed sections that significant advances in understanding have been made.

Heating of high-purity, electropolished aluminium specimens in air at temperatures around 500 °C for a short period, i.e. 10 min, results in surface coverage with a thin thermal oxide layer, about 5 nm thick, which is largely amorphous. Close scrutiny reveals the presence of fine γ-alumina crystals, a few nanometres in size, which can be detected only by transmission electron microscopy of the stripped oxide (Shimizu *et al.* 1991*a*). If the thermally oxidized specimens are anodized subsequently in a barrier forming electrolyte, such as an ammonium pentaborate solution, under the usual conditions, the development of lens-shaped γ'-alumina islands is observed within the otherwise amorphous barrier oxide films (figure 7). The diameter of the γ'-alumina islands increases linearly with increase in forming voltage as the barrier oxide thickens. These crystals are located near the middle of the barrier oxide films. Voids are normally present above, but adjacent to, the crystalline islands; the voids are filled with oxygen gas, formed by the oxidation of oxygen ions constituting the oxide at the amorphous–crystalline boundary (Crevecoeur & de Wit 1987). Due to the presence of voids, ionic transport is inhibited in these local regions and the metal–oxide interface exhibits a ridged appearance. The growth of the crystalline islands is due to the

PHILOSOPHICAL TRANSACTIONS OF THE ROYAL SOCIETY A MATHEMATICAL, PHYSICAL & ENGINEERING SCIENCES

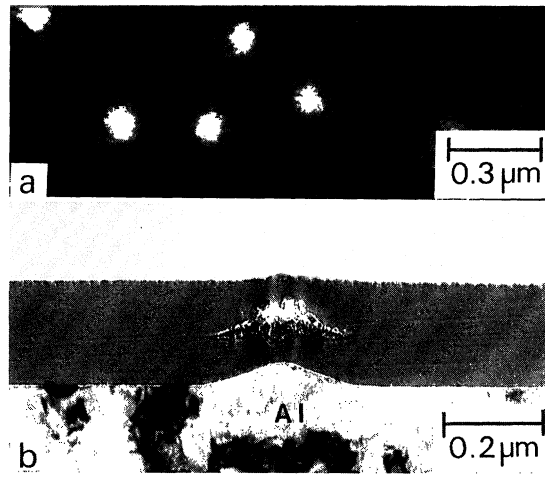

Figure 7. γ'-alumina crystals in a barrier oxide film formed on aluminium covered with a thin thermal oxide layer. (*a*) Stripped oxide film. (*b*) Cross-section. In the stripped film, γ'-alumina crystals appear as lighter, finely textured regions, about 300 nm in diameter. Here, an electropolished aluminium specimen was heated in air at 500 °C for 10 min and, subsequently, anodized at a constant current density of 5 mA cm^{-2} in 0.1 M ammonium pentaborate solution to 175 V.

presence, in the initial thermal oxide layer, of the fine γ-alumina crystals; these are incorporated within the growing barrier oxide. Further, the γ-alumina crystals act as nuclei for the amorphous to crystalline transformation, with the surfaces of the incorporated crystals providing stable lattice sites for Al^{3+} and O^{2-} ions migrating through the adjacent amorphous regions, as revealed in the schematic diagram of figure 8. The amorphous to crystalline transformation takes place during anodic oxide growth, in the presence of an electric field near 10^7 V cm^{-1}, and leads to the growth of γ'-alumina which is generally regarded as a less ordered form of γ-alumina, even though the initial nuclei for the transformation are γ-alumina crystals. Additionally, the interaction between the lattice sites and the migrating Al^{3+} and O^{2-} ions takes place preferentially at the crystal edges parallel to the direction of ionic movement for the amorphous oxide growth, and the transformation leads to the growth of lens-shaped γ'-alumina crystals extending laterally and parallel to the macroscopic surface of the metal. The voids observed above the islands arise from the development of the relatively compact γ' phase as a result of the amorphous to crystalline transformation.

From figure 8, it appears that the location of the γ'-alumina crystals, or the original γ-alumina crystals, in the anodic barrier oxide is determined by the transport numbers of the Al^{3+} and O^{2-} ions in the amorphous film during oxide growth. Conversely, from the location of the alumina crystals in the anodic barrier oxide, it should be possible to determine the transport numbers of the Al^{3+} and O^{2-} ions during the oxide growth. Thus the alumina crystals can be regarded here as structural markers for the determination of the transport numbers during oxide growth (Shimizu *et al.* 1991*b*). The determination of transport numbers is assisted by forming films to relatively low voltages, with the presence of relatively small, but detectable γ'-alumina crystals. This condition is closely met for the barrier oxide grown to 100 V, as shown in figure 9.

For the film formed to 100 V, the diameter of the γ'-alumina islands is approxi-

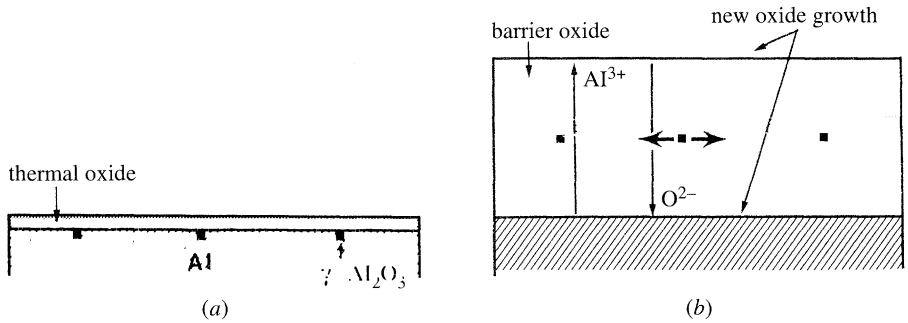

Figure 8. Schematic illustration representing the structure and growth of the barrier oxide on aluminium initially covered by a thin thermal oxide layer, with fine crystals of γ-alumina between it and the substrate.

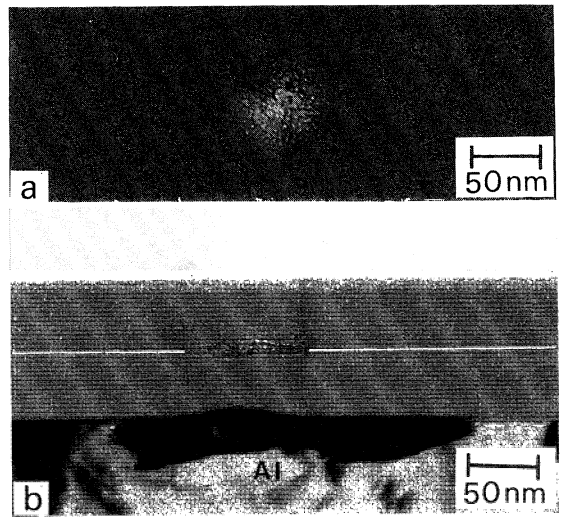

Figure 9. As figure 7, but formed to 100 V in order to determine the transport numbers from the location of the γ-alumina crystals.

mately 100 nm which is only one-third of that in the film formed to 175 V (figure 9*a*). However, a thin γ'-alumina crystal, with lateral dimensions of about 100 nm, is observed clearly within the normal amorphous barrier oxide and is located near the middle of the oxide (figure 9*b*). The thickness of the crystal is greatest, about 13 nm, at the central position, and the thickness decreases gradually and relatively symmetrically to about 7 nm towards the edges of the expanding crystal where the amorphous to crystalline transformation proceeds preferentially. Additionally, the formation of voids, which hinder ionic transport through local regions where the γ'-alumina islands are present, is not obvious as this stage. From the location of the initial γ-alumina crystal, which has been marked by a white line running parallel to the macroscopic surface of the metal, and allowing for the thickness of the initial amorphous thermal oxide, the transport number of Al^{3+} ions during the oxide growth is estimated to be 0.45, which agrees closely with that obtained by the usual ion-implanted xenon marker method. The agreement between the transport numbers obtained using entirely different kinds of markers confirms the immobility and the

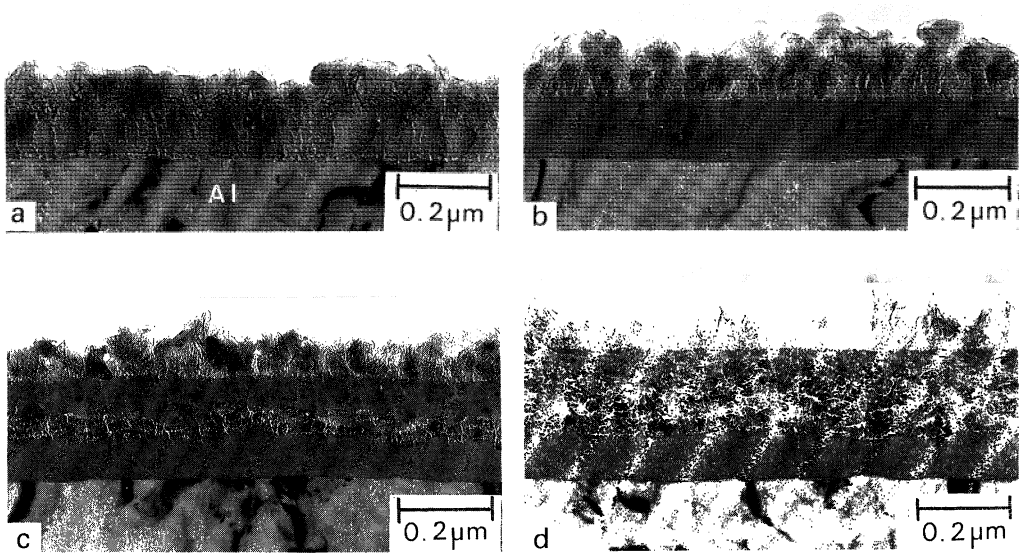

Figure 10. Transmission electron micrographs of ultramicrotomed sections of hydrous oxide film and composite barrier oxide films. (*a*) Hydrous oxide layer formed on electropolished aluminium specimens which were immersed in boiling distilled water for 5 min. (*b*) As in (*a*) after being anodized at a constant current density of 5 mA cm^{-2} in 0.1 M ammonium pentaborate solution to 100 V at 25 °C. (*c*) As in (*a*) and then anodized to 200 V. (*d*) As in (*a*) and then anodized to 300 V.

inertness of the ion-implanted xenon marker. The contribution, if any, of markers to oxide growth has been the subject of discussion since the marker approach was first introduced in 1965 by Davies *et al.* for the determination of the transport numbers during anodic oxide growth on so-called valve metals.

Immersion of high purity, electropolished specimens in boiling distilled water for a short period, for instance 5 min, results in rapid surface coverage with a relatively thin hydrous oxide film; the film consists of two distinct layers as shown in figure 10*a*. Adjacent to the metal, there is an inner dense, yet microporous, layer of relatively uniform thickness, about 110 nm, which consists of fine platelets of poorly crystallized pseudo-boehmite with sizes up to several nanometres. Above the inner layer, however, there is an outer fibrillar layer of varying thickness, which consists of randomly oriented and loosely connected platelets of relatively well crystallized pseudo-boehmite, of thickness less than 30 nm and lateral dimensions up to 150 nm. Such layered films are considered to develop from initial alumina gel-formation and subsequent dissolution/deposition processes. The detailed morphology of such films and the development of the pseudo-boehmite platelets have been described by Vedder & Vermilyea (1969).

During anodic oxidation of aluminium, covered with such a thin, microscopically porous hydrous oxide layer, in a barrier-forming electrolyte under the usual anodizing conditions, the growth of barrier oxide occurs. Growth proceeds both at the metal–oxide and the barrier oxide–hydrous-oxide interfaces by inward migration of O^{2-} and outward migration of Al^{3+} ions respectively, as shown schematically in figure 11. At the metal–oxide interface, amorphous oxide grows in the usual fashion by the inward migration of O^{2-} ions. However, at the barrier oxide–hydrous-oxide interface, amorphous oxide grows by the outward migration of Al^{3+} ions to fill the

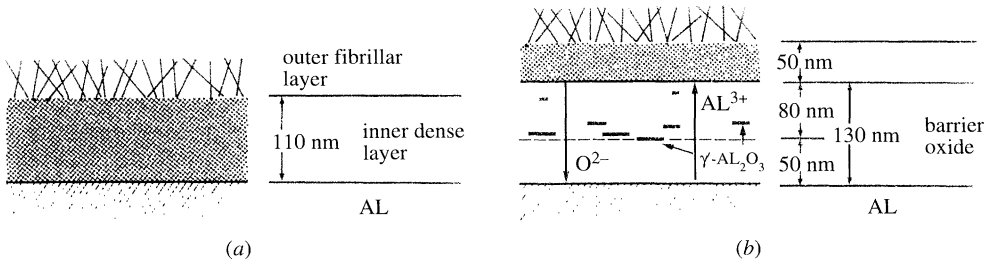

Figure 11. Schematic diagram of the structure and growth of barrier oxide film on aluminium initially covered with a hydrous oxide layer. (*a*) Hydrous oxide film. (*b*) Following anodizing to 100 V. This is a schematic picture of figure 10*b*. The dotted line represents the boundary separating the inner amorphous layer and the outer layer containing fine platelets of pseudo-boehmite.

channels or interstices of the inner relatively dense, yet porous, layer of hydrous oxide. Simultaneously, the inner layer of hydroxide becomes incorporated into the growing barrier oxide layer. As the barrier oxide grows thicker, more hydrous oxide is incorporated into the barrier oxide (figure 10*b*–*d*). For the barrier oxide formed to 300 V, the inner dense layer of hydrous oxide appears to have been almost completely incorporated into the barrier oxide (figure 10*d*). The fine platelets of poorly crystallized pseudo-boehmite incorporated into the barrier oxide are then subjected to the high electric field and dehydrate gradually to γ and γ'-alumina crystals which, in turn, act as nuclei for the amorphous to crystalline transformation. Stemming from this peculiar mode of the oxide growth, the barrier anodic oxide grown over the aluminium surface covered with a thin layer of hydrous oxide consists of two distinct layers: an inner amorphous oxide layer adjacent to the metal and an outer crystalline layer adjacent to the residual hydrous oxide layer. The crystallinity in the outer layer is greater at locations close to the inner layer where pseudo-boehmite crystals are initially incorporated into the barrier oxide. A network of fine cracks is normally observed in the outer, crystalline layer due to the volume contraction caused by the dehydration, under the high field, of the incorporated pseudo-boehmite crystals or by the amorphous to crystalline transformation. Such cracks, which are filled with oxygen gas, are a major cause of the electrical instability of electrolytic capacitors, generally called 'relaxation', which results in a sudden loss of the ability of the barrier oxide to sustain its original voltage. Thus the healing of these cracks is a major industrial requirement in the production of aluminium electrolytic capacitors with stable electrical performance.

Fundamental aspects of the growth of crystalline barrier oxide films on aluminium are now well understood. However, the practical situations are considerably more complex. In the industrial production of aluminium electrolytic capacitors, an aluminium foil is first treated by AC or DC etching in hydrochloric acid to increase its surface area. Etching with AC produces a fine, porous structure within the aluminium (figure 12*a*), which is suitable for the production of low-voltage type capacitors where the growth of relatively thin barrier oxide, normally less than 100 nm, is required. On the other hand, DC etching produces a characteristic tunnel-type structure (figure 12*c*), which is suitable for the production of high-voltage capacitors where the growth of thicker barrier oxide is required. In either case, the barrier oxide has to grow over convoluted aluminium surfaces under geometrical constraints. Furthermore, in the industrial production of electrolytic capacitors, anodizing is usually carried out at elevated solution temperatures, around 90 °C, to stimulate the growth of the crys-

PHILOSOPHICAL TRANSACTIONS OF THE ROYAL SOCIETY A MATHEMATICAL, PHYSICAL & ENGINEERING SCIENCES

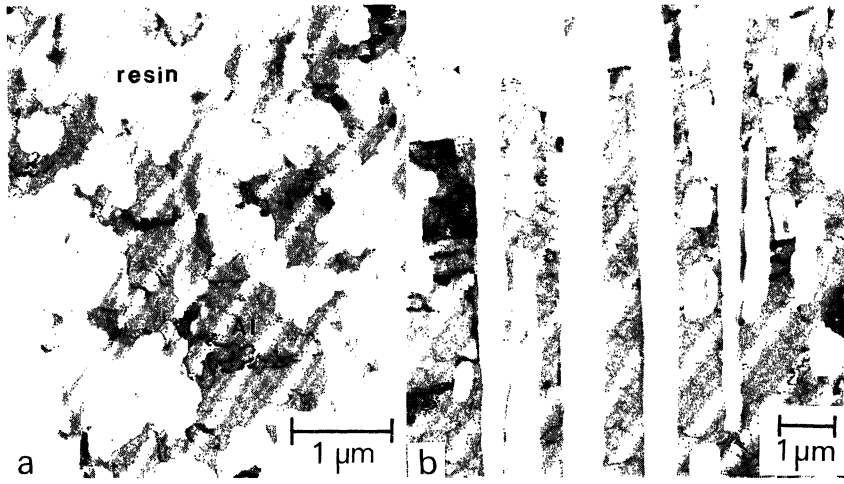

Figure 12. Transmission electron micrographs of ultramicrotomed sections of etched aluminium foils for capacitor applications. (*a*) An aluminium foil etched under AC conditions. (*b*) An aluminium foil etched by DC.

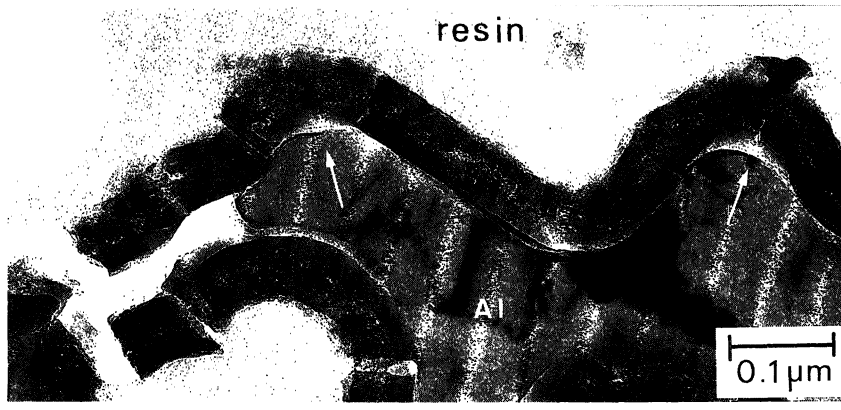

Figure 13. Transmission electron micrograph of an ultramicrotomed section of the barrier oxide film, formed on an AC etched aluminium foil.

talline oxide. Consequently the barrier oxide grown on the etched aluminium foils under industrial conditions is markedly different from that grown on the smooth, relatively electropolished aluminium surfaces used for fundamental studies.

In the capacitor industry there has been considerable interest in the structure of the barrier oxide grown by anodizing on etched aluminium foils of geometry shown in figure 13, because the electrical stability of the capacitors depends critically upon the nature of defects in the barrier oxide. Scanning electron microscopy of fracture sections is used routinely for examination. However, due to the limited resolution of the technique, the structure of the barrier oxide has remained largely uncertain before the application of transmission electron microscopy of ultramicrotomed sections (Shimizu *et al.* 1992).

Figure 13 shows a transmission electron micrograph of an ultramicrotomed section of a low-voltage-type capacitor foil anodized under an industrial condition. Ultramicrotomed sections of 10 nm thickness can be prepared successfully for the etched

and, subsequently, anodized aluminium foils of complex porous structures. The barrier oxide is observed clearly as a dark band of material over the convoluted surfaces of the etched aluminium foil. The barrier oxide is about 55 nm thick and reveals a two-layered structure. Adjacent to the metal, there is an inner amorphous layer, about 15 nm thick, which appears featureless. Above the inner layer and adjacent to the embedding epoxy resin, there is an outer, crystalline layer about 40 nm thick. Selected area electron diffraction analysis of the barrier oxide has shown that it consists of amorphous oxide and γ'-alumina crystals. Numerous fine voids, a few nanometres in diameter, are observed in the outer crystalline layer. As described previously, these voids are inherent structural defects associated with the crystalline oxide. It appears that they are present as discrete voids, or as connected voids, with the latter forming a network of fine channels or cracks within the outer crystalline layer.

In addition to the voids and network of cracks, which are inherent structural defects associated with the crystalline barrier oxide, transmission electron microscopy of ultramicrotomed sections successfully reveals other defects, which arise from the growth of the irregularly shaped etched aluminium surfaces. Naturally, such defects are found only in the barrier oxide grown on the etched aluminium foils and are observed normally at the corners of the curved aluminium surface where greater stress development is expected within the growing barrier oxide. Depending on the extent of local curvature of the aluminium surface in these local regions, they occur as (*a*) vertical cracks extending to the metal–oxide interface; (*b*) local regions where the barrier oxide appears to have been detached from the substrate; (*c*) local regions where the growth of continuous barrier oxide is hindered. The defects of type (*a*) and (*b*) are observed clearly in figure 13 at the locations indicated by the arrows.

Of the various defects described, the network of cracks observed in the outer crystalline layer are the main cause of the characteristic instability of the electrolytic capacitor, the so-called relaxation. Defects of type (*c*) provide preferential sites for breakdown, thereby limiting the operational voltage of the capacitors to a level considerably lower than expected from the barrier oxide thickness during the anodization process. Defect type (*b*) is also detrimental, since it provides potential sites which could eventually lead to local spalling of the barrier oxide.

4. Surface films on heterogeneous metal surfaces

Controversy has arisen in the past over whether the Al_3Fe particles (constituents of many commercial aluminium alloys) are oxidized, dissolved or incorporated into porous anodic oxides during anodic oxidation of Al–Fe alloys in sulphuric acid solutions (Zahavi *et al.* 1978). Such controversy is resolved readily by transmission electron microscopy of ultramicrotomed sections of the aluminium substrate and its porous oxide film. Figure 14 shows the sectional appearance of an Al–1.5 wt%Fe alloy after anodizing at a constant current density of 5 mA cm^{-2} in 2.4 M sulphuric acid at 25 °C for 2 min. Fine Al_3Fe particles of sizes up to a few microns are observed clearly within the aluminium-rich matrix. Such particles are readily differentiated from the surrounding matrix because of their greater electron scattering cross-section and deformation characteristics during sectioning. They appear to have been subjected to more irregular parting during slicing, evident as narrow and relatively equally spaced 'chatter bands' running perpendicular to the direction of cutting. Porous oxide growth is evident not only over the aluminium matrix surface, surrounding finely dispersed Al_3Fe particles, but also over the surfaces of the Al_3Fe particles protrud-

PHILOSOPHICAL TRANSACTIONS OF THE ROYAL SOCIETY A MATHEMATICAL, PHYSICAL & ENGINEERING SCIENCES

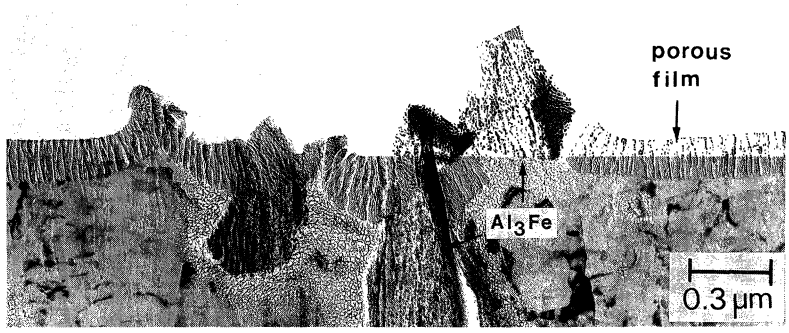

Figure 14. Transmission electron micrograph on an ultramicrotomed section of the porous oxide film grown in an Al–1.5 wt% Fe alloy at a constant current density of 5 mA cm^{-2} in 2.4 M sulphuric acid at 25 °C for 2 min.

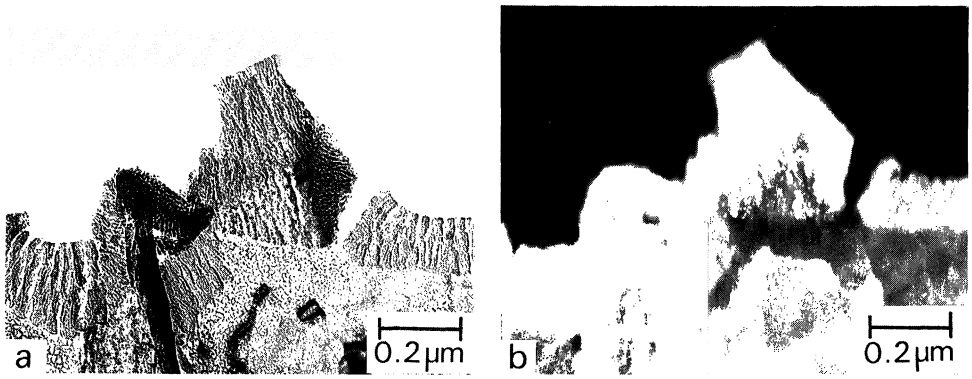

Figure 15. Enlargement of a local area in figure 14. (*a*) Bright field micrograph. (*b*) Micrograph revealed by crudely displacing the objective aperture from the transmitted beam location.

ing from the initial aluminium surface. Porous oxide growth over the Al_3Fe particle is observed more clearly in figure 15*a*, which is an enlargement of a local area in figure 14, where an Al_3Fe particle of a triangular shape is present at the aluminium surface. Additionally, the boundary between the porous oxide and the Al_3Fe phase is revealed clearly in figure 15*b*, which was obtained crudely by moving the objective aperture away from the transmitted beam location to a diffraction spot arising from the crystalline second phase material. It is now evident that the Al_3Fe particles are oxidized during anodizing in sulphuric acid, forming a porous-type oxide similar to that on the aluminium matrix. However, the composition of the oxide is different. EDX analysis has shown that the oxide grown over the Al_3Fe particles contains iron along with oxygen, aluminium, and sulphur, which are detected in the normal porous oxide grown over the aluminium matrix surface. Further, the differential rates of growth of the oxide over the matrix and second phase matrix, influenced possibly by preferential leaching of iron species from the barrier layer oxide and, possibly, changes in its ionic conductivity due to incorporation of iron species, generates complex interfacial geometries at the matrix–Al_3Fe boundaries.

As clearly shown by this example, one of the most important advantages of the cross-sectional transmission electron microscopy is that it allows one-to-one correspondence to be made between the microscopical heterogenities of the metal surface and local film character. Additionally and importantly, recent studies on the growth

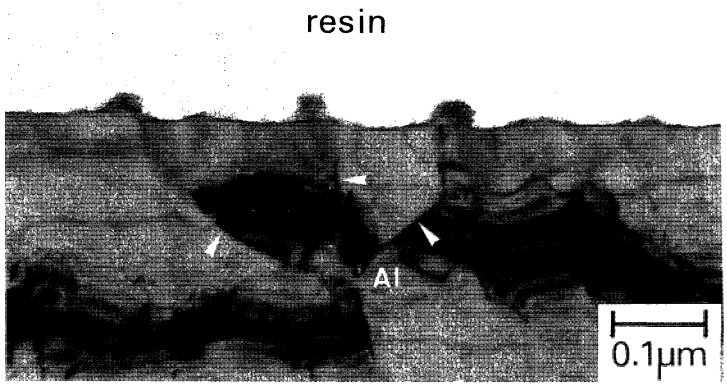

Figure 16. Transmission electron micrograph of an ultramicrotomed section of an electropolished, high purity, aluminium specimen which was immersed for 5 s in an acid chromate chemical conversion coating bath.

of chromate chemical conversion coatings on high purity aluminium have shown that transmission electron microscopy of ultramicrotomed sections allows direct correlation to be made between the local film character and much finer heterogenities of the metal surface, such as grain boundaries or cellular boundaries, which are now considered further (Brown *et al.* 1992).

The treatment of aluminium by immersion in acid chromate solutions is often used to produce protective coatings on the metal surface. The resultant chemical conversion coatings are of great practical importance since they increase the corrosion resistance of the metal and also act as keying layers to promote adhesion between the metal and subsequently applied organic coatings, such as paints. While chemical conversion coating is widely used, the development and growth of the coatings have remained largely unclear until recently. In order to understand their mechanism of growth, it is important to note that various electrochemical processes proceed over the aluminium surface which is generally covered with a thin, insulating passive oxide layer, normally a few nanometres thick. However, the passive films are not continuous, but always contain defects or 'flaws' due to surface heterogenities associated with impurity segregation within the metal. Further, even for aluminium specimens of 99.99% purity, the relatively small amount of impurities are not distributed uniformly throughout the aluminium matrix, but segregate into thin, three-dimensional and continuous regions enclosing small volumes of relatively high-purity aluminium, giving a so-called 'cellular honeycomb' structure (Cuff & Grant 1958). The regions where the grain boundaries or cellular boundaries intersect the aluminium surface constitute minor surface heterogenities. Consequently, flaws are formed in the passive oxide layer at such surface heterogenities and play an important role in the development of chemical conversion coatings, since they provide easy paths for electronic conduction in the otherwise insulating passive oxide layer.

During chromate conversion coating growth on high purity aluminium, the anodic reaction, i.e. the growth of an aluminium oxide film, with subsequent chemical dissolution by HF (a component of the conversion coating solution), occurs over the aluminium surface. The conversion coating growth, as a result of the cathodic reduction of dichromate to hydrated chromium oxide species, takes place preferentially along the flaw sites which provide easy paths for electronic conduction.

Figure 16 shows a transmission electron micrograph of an ultramicrotomed section of an electropolished, high purity aluminium specimen which was given a chemical conversion coating treatment for 5 s in a bath containing 4 g l^{-1} CrO3, 3.5 g l^{-1} $Na_2Cr_2O_7$ and 0.8 g l^{-1} NaF at 298 K. The aluminium substrate is observed at the bottom of the micrograph and the embedding resin is observed at the top of the micrograph . The hydrated chromium oxide appears as dark spots, about 20–30 nm in size, which are sited at the top of the ridged aluminium surface. It is immediately evident that the deposits of conversion coating are sited at the locations where the cellular boundaries intersect the surface. This confirms that the cellular structure within the aluminium and the boundaries, enveloping the cells, represent regions of impurity segregation.

5. Electrodeposited Ni–P alloys

Electrodeposition is one of the most popular methods for the preparation of amorphous metallic alloys. The method is technically simple and generally inexpensive; it is able to provide coatings rapidly and it is well suited for coating of large areas, including complex shapes of industrial interest. In the structural analysis of the deposit by X-ray related techniques (Cargill 1970, 1975), it is generally assumed that the deposits are uniform across the film thickness. However, this is not always the case (Shimizu *et al.* 1990*b*). As clearly shown in figure 17, an electrodeposited Ni–P alloy of relatively low phosphorus content, for example Ni_{86}–P_{14}, consists of fine layers of differing phosphorus contents and crystallinity. This is due to the systematic fluctuation of pH at the alloy–electrolyte interface during electrodeposition which, in turn, affects the reduction of phosphorus acid to phosphorus, through hypophosphite (Chen *et al.* 1988). Conversely, an electrodeposited Ni–P alloy of high phosphorus content, for example Ni_{77}–P_{23}, appears featureless and uniform in contrast in the electron microscope (figure 18*a*). No layered structure, associated with the difference in phosphorus content and, hence, crystallinity, is observed. Further examination at high resolution indicates that the alloy is largely amorphous, except for the occasional presence of ordered regions, a few nanometres in diameter (figure 18*b*) suggesting that the structure of the alloy may not be represented by a simple DRP model as suggested by Cargill. Further evidence for the complexity of the structure of the alloy is obtained by Fourier transformation of the high resolution image, which was acquired digitally. The Fourier transform of a local area, shown in figure 19*a*, is revealed in figure 19*b*. The diffraction spots arise from (111) fringes of the copper substrate. Diffuse haloes, around the diffraction spots, result from Ni_{77}–P_{23} alloy. The diffuse halo is relatively uniform, but exhibits certain orientation, suggesting that the structure of the alloy is more complex than previously thought. Such complexity may be associated with the electrodeposition process, but the details require further investigation. In addition, the detailed interpretation of the Fourier transform of the image requires careful consideration since effects relating to the transfer characteristics of the electron microscope objectives lens may give rise to diffuse haloes. Further, the surfaces of the ultramicrotomed sections of the metals/alloys are covered by relatively thin air-formed films which may contribute to the contrast revealed.

Thus it has been generally agreed that electrodeposited Ni–P alloys are crystalline at lower phosphorus content. However, as the phosphorus content increases, the size of the nickel crystals decreases and, at a phosphorus content of about 18 at.%, the al-

PHILOSOPHICAL TRANSACTIONS OF THE ROYAL SOCIETY A MATHEMATICAL, PHYSICAL & ENGINEERING SCIENCES

Figure 17 Figure 18

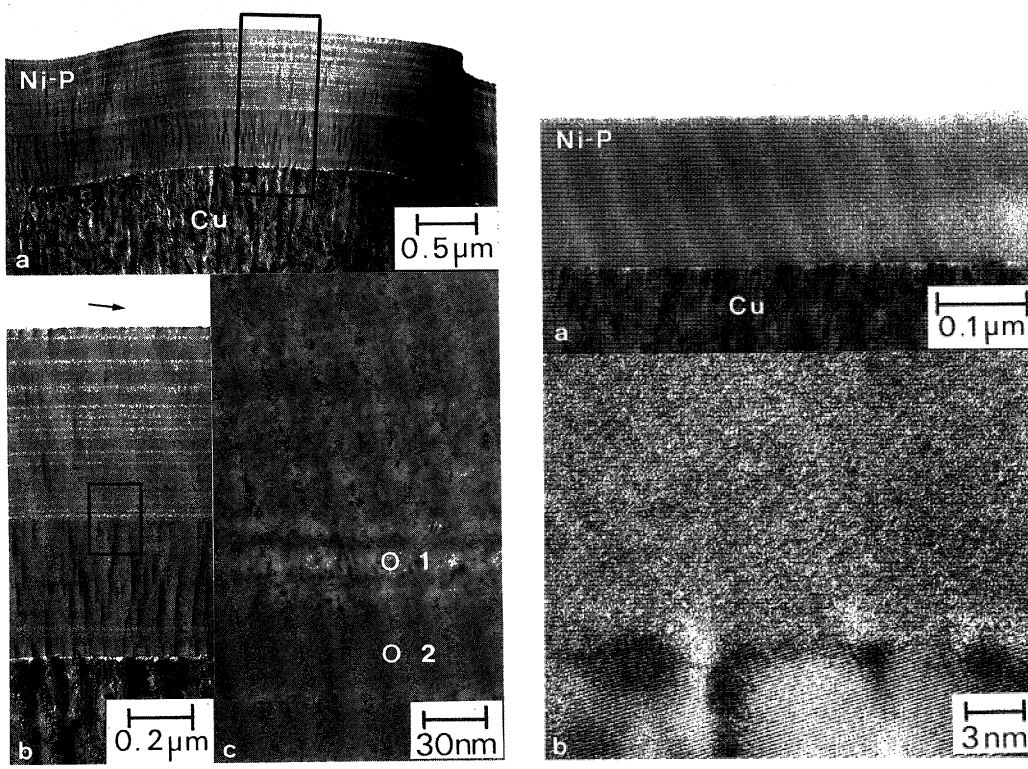

Figure 17. Transmission electron micrograph of an ultramicrotomed section of Ni_{86}–P_{14} alloy, showing the presence of fine layers of different crystallinity. The alloy was electrodeposited from a nickel sulphate, nickel chloride, boric acid and phosphoric acid mixture, using a current density of 5 A dm^{-2} at 70 °C for 1 min. (*a*) General view. (*b*) An enlargement of the boxed area shown in (*a*). (*c*) An enlargement of the boxed area shown in (*b*). EDX analysis of local areas shown in (*c*) indicates that the phosphorus content in probe position (1) is less than in probe position (2).
Figure 18. Transmission electron micrograph of an ultramicrotomed section of Ni_{77}–P_{23} alloy. (*a*) General view. (*b*) High resolution image, showing the presence of an 'ordered region', a few nanometres in size, in the alloy.

loy becomes essentially amorphous (McMahon & Erb 1989). In the previous studies, the structure of the electrodeposited Ni–P alloys was determined largely by X-ray diffraction. From the width of the diffraction peaks, the size of nickel crystals was determined using the Debye–Scherrer equation. Compositional and structural uniformity of the alloys were implicity assumed. However, as shown here, the electrodeposited Ni–P alloys are not always uniform in composition and structure throughout the film thickness. Cross-sectional transmission electron microscopy provides essential insight into the complex processes associated with the crystalline to amorphous transformation in the electrodeposited Ni–P alloys.

6. Thermal oxide films on copper

The thermal oxidation of copper is a system which has been investigated extensively to understand the fundamental aspects of metal oxidation (Young *et al.* 1956;

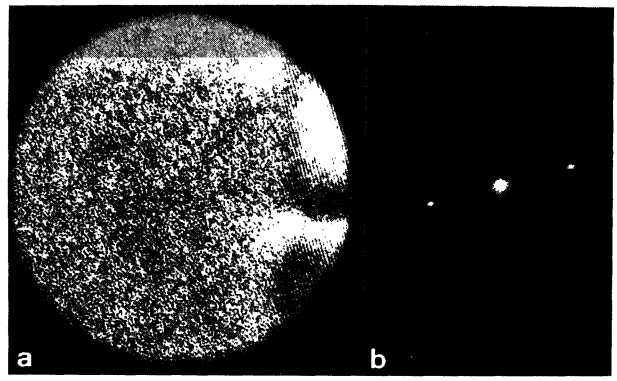

Figure 19. (*a*) Local area in figure 18*b*. (*b*) Fourier transform obtained from the local area shown in (*a*).

Lawless & Gwathmey 1956; Cathcart & Peterson 1968). The thermal oxide films on copper are crystalline and have a 'mosaic' structure due to the epitaxial interactions between the metal and the oxide. Additionally, short-circuit diffusion through the boundaries between the mosaic blocks of crystallites is considered to be the predominant mode of materials transport during the oxide growth. Since the epitaxial relationships are different for different crystal faces, corresponding variations are expected in the mosaic structure which, in turn, lead to the marked differences in the oxidation rates exhibited by different crystal faces. Thus detailed information on the structure of the oxide is essential for understanding oxide growth processes on copper.

Electropolished, polycrystalline copper, oxidized in purified oxygen at 178 °C for 10 min, is amenable to high resolution transmission electron microscopy of ultramicrotomed sections, where the structure of the oxide grown over grains of different orientations has been revealed at atomic scale resolution. This allows direct correlation between the density of paths for easy diffusion in the oxide and oxidation rates (Shimizu *et al.* 1996 (unpublished work)). From such observations it is evident that the oxide growth processes are considerably more complex than previously interpreted. In particular, the fate of vacancies, left in the metal as metal atoms are preferentially injected into the oxide through local sites, where the paths for easy diffusion in the oxide meet the metal substrate, and how direct contact can be maintained between the metal and oxide at such local regions during the oxide growth require clarification.

Perhaps, these questions are best addressed by examination of the oxide grown on the (111) face of copper, since the nature of 'incoherent' boundaries in the oxide, which act as paths for easy diffusion, can be specified uniquely at the metal–oxide interface. For the (111) face, where the epitaxial relationship between the oxide and metal is represented by $(111)Cu_2O \| (111)Cu$, oxide nuclei may be formed with two different, but energetically equivalent orientations, i.e. parallel or antiparallel orientations. In the former, the oxide lattice is essentially parallel to that of the metal; in the latter, the oxide lattice is rotated 180° about its surface normal to produce the antiparallel orientation. Thus on the (111) face, two adjacent oxide nuclei may have different orientations, the parallel and the twin-related antiparallel orientations, forming a so-called 'incoherent' boundary which acts as a path for easy diffusion.

Figure 20. Transmission electron micrograph of an ultramicrotomed section of the thermal oxide film grown on the (111) face of copper which has been oxidized in purified oxygen at 178 °C for 10 min.

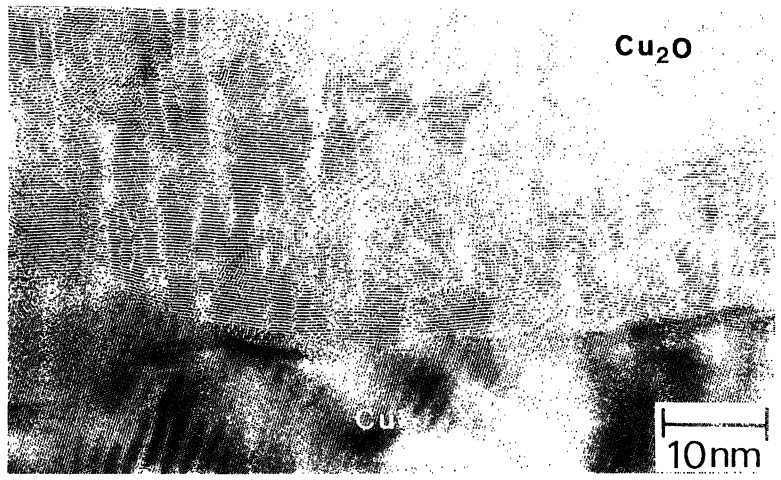

Figure 21. High resolution image of the copper–oxide interface, revealing the epitaxial interaction between the metal and oxide and consequent development of the mosaic structure in the oxide.

Figure 20 shows a transmission electron micrograph of an ultramicrotomed section of the copper substrate and its oxide grown on the (111) face by heating in purified oxygen of approximately 1 atm† at 178 °C for 10 min. Examination of the copper sections reveals that its surface has been oriented precisely to (111). The Cu_2O film of relatively uniform thickness, about 40 nm, is present at the surface; the micrograph also reveals the relatively extensive interfacial region generated by ultramicrotomy.

Figure 21 shows an enlargement of a local area of figure 20. The metal–oxide interface and the mosaic structure of the oxide are revealed clearly with atomic scale resolution. It appears that the (111) planes in the oxide run approximately parallel to the macroscopic surface of the metal. However, it is evident that the oxide–metal interface is not atomically flat over an extended distance, i.e. 1 mm, which is considerably greater than the sizes of Cu_2O crystals constituting the oxide film. Such

† 1 atm $\approx 10^5$ Pa.

PHILOSOPHICAL TRANSACTIONS OF THE ROYAL SOCIETY A MATHEMATICAL, PHYSICAL & ENGINEERING SCIENCES

a roughness of the metal–oxide interface is not just restricted to the local region indicated in the micrograph, but is also observed generally. Additionally, and at local regions where the metal–oxide interface exhibits curvature, narrow, relatively equally spaced, and slightly tilted boundaries are observed within the oxide close to the metal–oxide interface. Such boundaries run approximately perpendicular to the macroscopic surface of the metal. At this stage, details of the mechanism of the formation of such boundaries and their implications on the microscopic processes of ionic migration involved in oxide growth on copper have yet to be determined. Nevertheless, the enormous potential of transmission electron microscopy of ultramicrotomed sections has been clearly demonstrated here.

7. Conclusions

In the present paper the impact and scope of modern transmission electron microscopy in the examination of amorphous and crystalline films, including amorphous to crystalline and reverse transformations, have been highlighted. Ultramicrotomy is a particularly successful specimen preparation route for the relatively thin films of interest in corrosion studies. The tremendous range of resolution of electron microscopy provides general and local information which is essential to the understanding of the general properties and local specific features of the film of interest. Further, the direct observation approach, with related elemental and structural analyses, does not require inferences to be made and provides very precise and quantitative information relating to the highlighted amorphous and crystalline films and transformations proceeding during film growth under particular conditions.

The approach is also successful in situations where the metal substrates are relatively hard and tough, e.g. zirconium (Kurima 1993), titanium (Shimizu *et al.* 1996 (unpublished work)) and stainless steels (Furneaux *et al.* 1978).

Thanks are due to the Royal Society and the Science and Engineering Research Council (UK) for the provision of a Guest Research Fellowship and a Senior Visiting Fellowship respectively to K.S.

References

Brown, F. & Mackintosh, W. D. 1973 The use of Rutherford backscattering to study the behaviour of ion implanted atoms during anodic oxidation of aluminium: Ar, Kr, Xe, K, Rb, Cs, Cl, Br and I. *J. Electrochem. Soc.* **120**, 1096–1102.

Brown, L. M. 1988 Microdiffraction. *Inst. Phys. Conf. Ser. 93*, **2**, 1–8.

Brown, G. M., Shimizu K., Kobayashi K., Thompson, G. E. & Wood, G. C. 1992 The morphology, structure and mechanism of growth of chemical conversion coatings on aluminium. *Corros. Sci.* **33**, 1371–1385.

Cargill, G. S. 1970 Structural investigation of noncrystalline nickel–phosphorus alloys. *J. Appl. Phys.* **41**, 12–29.

Cargill, G. S. 1975 Structure of metallic alloy glasses. *Solid State Phys.* **30**, 227–320.

Cathcart, J. V. & Petersen, G. E. 1968 Structural characteristics of the oxide on the (111) surface of copper. *J. Electrochem. Soc.* **115**, 595–597.

Chen, S., Yin, K. M. & White, R. E. 1988 A mathematical model for the electrodeposition of alloys on a rotating disk electrode. *J. Electrochem. Soc.* **135**, 2193–2200.

Crevecoeur, C. & de Wit, H. J. 1974 The growth of anodic aluminium oxide layers after a heat-treatment. *J. Electrochem. Soc.* **121**, 1465–1474.

Crevecoeur, C. & de Wit, H. J. 1987 The anodization of heated aluminium. *J. Electrochem. Soc.* **134**, 808–816.

Cuff, B. E. & Grant, J. 1959 A segregation substructure in aluminium. *J. Inst. Met.* **87**, 248–254.

Davies, J. A., Domeij, B., Pringle, J. P. S. & Brown, F. 1965 The migration of metal and oxygen during anodic film formation. *J. Electrochem. Soc.* **112**, 675–680.

Dell'Oca, C. J. & Young, L. 1970 High-field ionic conduction in tantalum anodic oxide films with incorporated phosphate. *J. Electrochem. Soc.* **117**, 1548–1551.

Dignam, M. J. 1972 *Oxides and oxide films* (ed. J. W. Diggle), vol. 1, pp. 96–286. New York: Marcel Dekker.

Furneaux, R. C., Thompson, G. E. & Wood, G. C. 1981 The coloured film formed on stainless steel in hot chromic/sulphuric acid solution. *Corros. Sci.* **21**, 23–29.

Kerr, I. S. 1956 Structure and crystallization of newly amorphous beryllium oxide and aluminium oxide films. *Acta Crystallogr.* **9**, 879–885.

Kobayashi, K. & Shimizu, K. 1986 Crystalline barrier oxide films on aluminium. In *Aluminium surface treatment technology* (ed. R. S. Alwitt & G. E. Thompson), pp. 380–393. Princeton NJ: The Electrochemical Society.

Kurima, Y. 1993 The anodic oxidation behaviour of chemically polished and electropolished zirconium. Ph.D. thesis, University of Manchester.

Lawless, K. R. & Gwathmey, A. T. 1956 The structure of oxide films on different faces of a single crystal of copper. *Acta Metall.* **4**, 153–163.

McMahon, G. & Erb, U. 1989 Structural transitions in electroplated Ni–P alloys. *J. Mater. Sci. Lett.* **8**, 865–868.

Pringle, J. P. S. 1973*a* The migration of oxygen during the anodic oxidation of tantalum. *J. Electrochem. Soc.* **120**, 1391–1400.

Pringle, J. P. S. 1973*b* Transport numbers of metal and oxygen during the anodic oxidation of tantalum. *J. Electrochem. Soc.* **120**, 398–407.

Randall, J., Bernard, W. J. & Wilkinson, R. R. 1965 A radiotracer study of the composition and properties of anodic oxide films on tantalum and niobium. *Electrochim. Acta* **10**, 183–201.

Shimizu, K., Thompson, G. E. & Wood, G. C. 1981*a* Direct observation of the duplex nature of anodic barrier films on aluminium. *Thin Solid Films* **81**, 39–44.

Shimizu, K., Thompson, G. E. & Wood, G. C. 1981*b* Electron-beam-induced crystallization of anodic barrier films on aluminium. *Thin Solid Films* **77**, 313–318.

Shimizu, K., Thompson, G. E., Wood, G. C. & Xu, Y. 1981*c* Direct observations of ion-implanted xenon marker layers in anodic barrier films on aluminium. *Thin Solid Films* **88**, 255–262.

Shimizu, K., Thompson, G. E., Wood, G. C., Kurima, Y. & Kobayashi, K. 1989 Direct observation of the two-layer structure of anodic oxide films on tantalum. *Phil. Mag.* A **60**, 591–596.

Shimizu, K., Thompson, G. E., Wood, G. C. & Kobayashi, K. 1990*a* Structural ordering in annealed anodic oxide films on aluminium. *Phil. Mag. Lett.* **61**, 133–138.

Shimizu, K., Thompson, G. E., Wood, G. C. & Kobayashi, K. 1990*b* Cross-sectional transmission electron microscopy of electrodeposited Ni–P alloys. *Phil. Mag. Lett.* **61**, 43–48.

Shimizu, K., Kobayashi, K., Thompson, G. E. & Wood, G. C. 1991*a* The apparent induction period for γ-Al_2O_3 development in thermal oxide films on aluminium. *Oxid. Met.* **36**, 1–13.

Shimizu, K., Kobayashi, K., Thompson, G. E. & Wood, G. C. 1991*b* A novel marker for the determination of transport numbers during anodic barrier-type oxide growth on aluminium. *Phil. Mag.* B **64**, 345–353.

Shimizu, K., Thompson, G. E., Wood, G. C. & Kobayashi, K. 1991*c* Microcrystallinity in X-ray amorphous anodic Ta_2O_5 films. *Phil. Mag.* B **63**, 891–899.

Shimizu, K., Kobayashi, K., Thompson, G. E. & Wood, G. C. 1992 The nature and origin of defects in the barrier oxide layers grown on etched aluminium foils for capacitor applications. *J. Mater. Sci. Lett.* **11**, 281–283.

Skeldon, P., Shimizu, K., Thompson, G. E. & Wood, G. C. 1985 Fundamental studies elucidating anodic barrier-type film growth on aluminium. *Thin Solid Films* **123**, 127–133.

Skeldon, P., Shimizu, K., Thompson, G. E. & Wood, G. C. 1994 Mobile tracers: their use in understanding key features of anodic alumina film formation. *Phil. Trans. R. Soc. Lond.* A **348**, 295–314.

PHILOSOPHICAL TRANSACTIONS OF THE ROYAL SOCIETY A MATHEMATICAL, PHYSICAL & ENGINEERING SCIENCES

Thompson, G. E., Xu, Y., Han, H. S., Skeldon, P., Shimizu, K. & Wood, G. C. 1987 Anodic oxidation of aluminium. *Phil. Mag.* B **55**, 651–667.

Thompson, G. E., Shimizu, K., Bethune, B. & Wood, G. C. 1991 Materials' ultramicrotomy in corrosion science. *Microsc. Analysis*, Sept., pp. 41–43.

Timsit, R. S., Waddington, W. G., Humphreys, C. J. & Hutchison, J. L. 1985*a* Structure of the aluminium/aluminium oxide interface. *Appl. Phys. Lett.* **46**, 830–832.

Timsit, R. S., Waddington, W. G., Humphreys, C. J. & Hutchison, J. L. 1985*b* Examination of the aluminium/alumina interface by high-resolution electron microscopy. *Ultramicroscopy* **18**, 387–394.

Vedder, W. & Vermilyea, D. A. 1969 Aluminium + water reaction. *Trans. Faraday Soc.* **65**, 561–584.

Vermilyea, D. A. 1957 Ionic conductivity of anodic films at high field strengths: transient behaviour. *J. Electrochem. Soc.* **104**, 427–433.

Verwey, E. J. W. 1935 Electrolytic conduction of a solid insulator at high voltages – formation of the anodic oxide film on aluminium. *Physica* **2**, 1059–1063.

Young, L. 1960 Steady-state kinetics of formation of anodic oxide films on tantalum in sulphuric acid. *Proc. R. Soc. Lond.* A **258**, 496–515.

Young, L. 1961 *Anodic oxide films*. New York: Academic Press.

Young, F. W., Cathcart, J. V. & Gwathmey, A. T. 1956 The rate of oxidation of several faces of a single crystal of copper as determined with elliptically polarized light. *Acta Metall.* **4**, 145–152.

Zahavi, J., Zangvil, A. & Metzger, M. 1978 Structure and stability of anodic films formed on aluminium containing dispersed Al_3Fe phase. *J. Electrochem. Soc.* **125**, 438–444.

Received 11 February 1994; accepted 19 April 1995

PHILOSOPHICAL TRANSACTIONS OF THE ROYAL SOCIETY A MATHEMATICAL, PHYSICAL & ENGINEERING SCIENCES

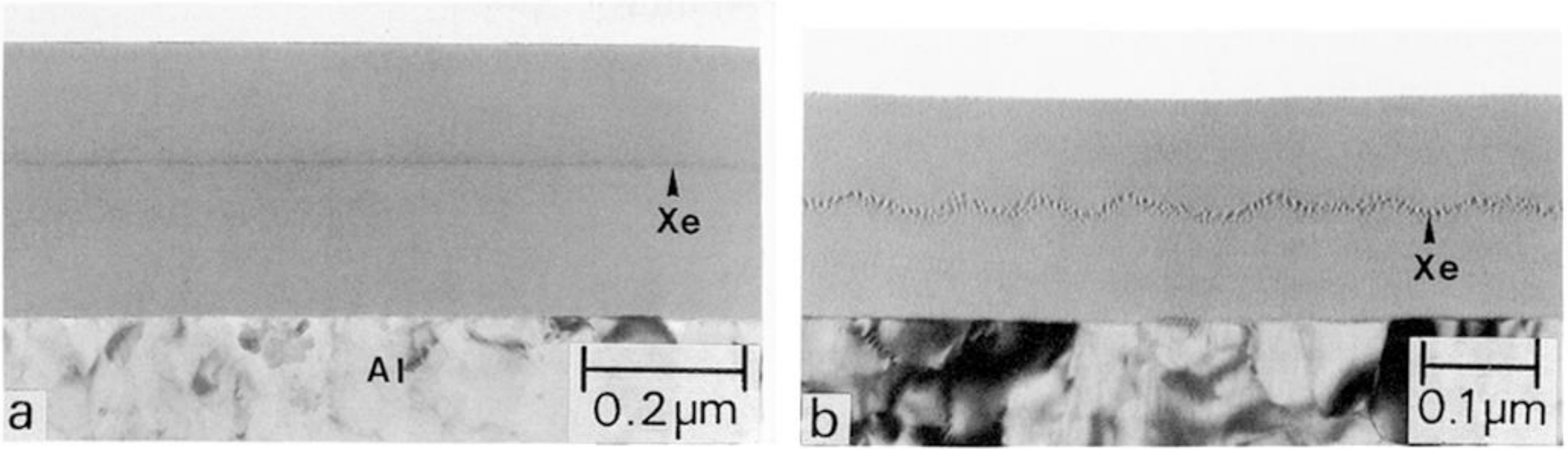

Figure 1. Xenon marker layers in barrier oxide films formed on aluminium in different electrolytes, after a thin pre-formed layer was implanted with xenon marker. (*a*) Film formed at a constant current density of 2 mA cm^{-2} in 5 wt% ammonium pentaborate solution to 300 V at 3 °C. (*b*) Film formed at a constant current density of 10 mA cm^{-2} in a borate-glycol electrolyte to 180 V at 25 °C.

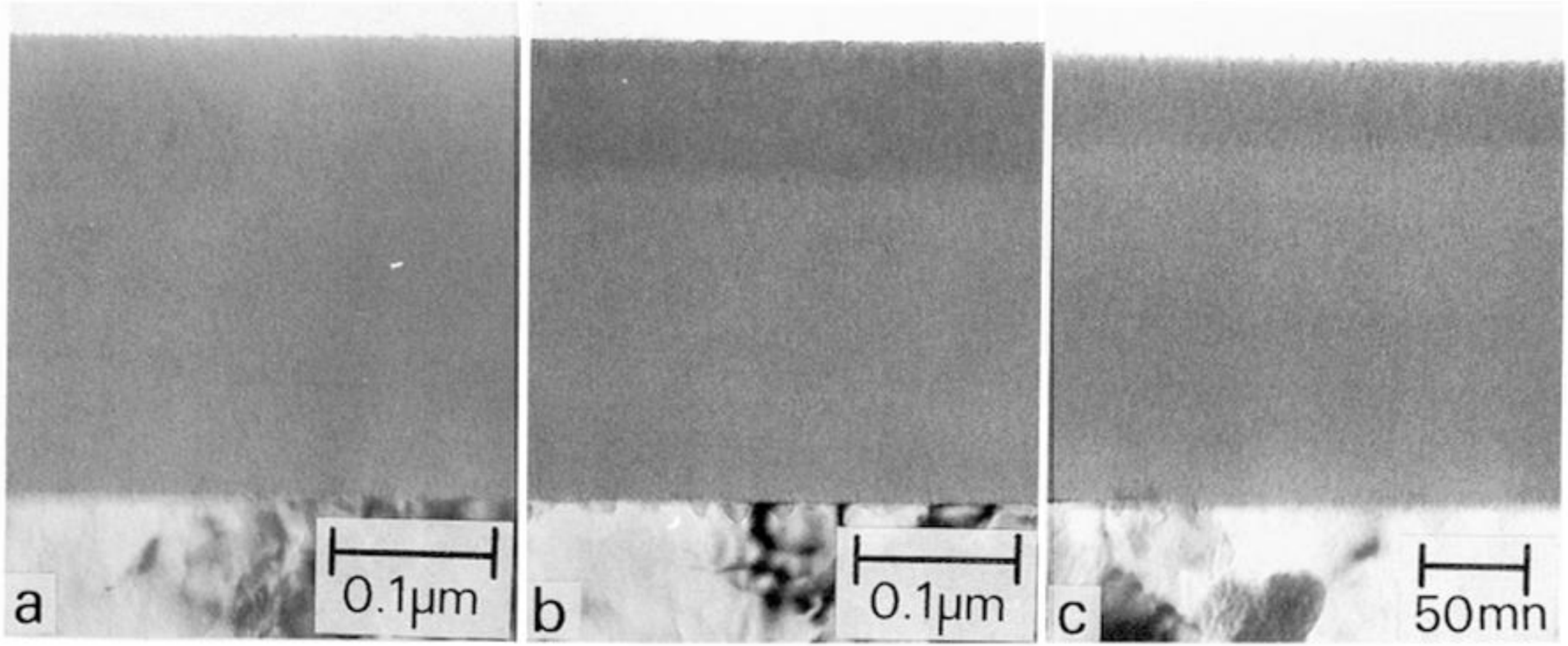

igure 2. Transmission electron micrographs of ultramicrotomed sections of barrier oxide films ormed on aluminium in different electrolytes. The films were formed at a constant current ensity of 5 mA cm^{-2} in 0.1 M solutions of the respective electrolytes at 25 °C. (*a*) Film formed t 300 V in an ammonium pentaborate solution. (*b*) Film formed to 250 V in a sodium tungstate olution. (*c*) Film formed to 175 V in a sodium molybdate solution.

Figure 3

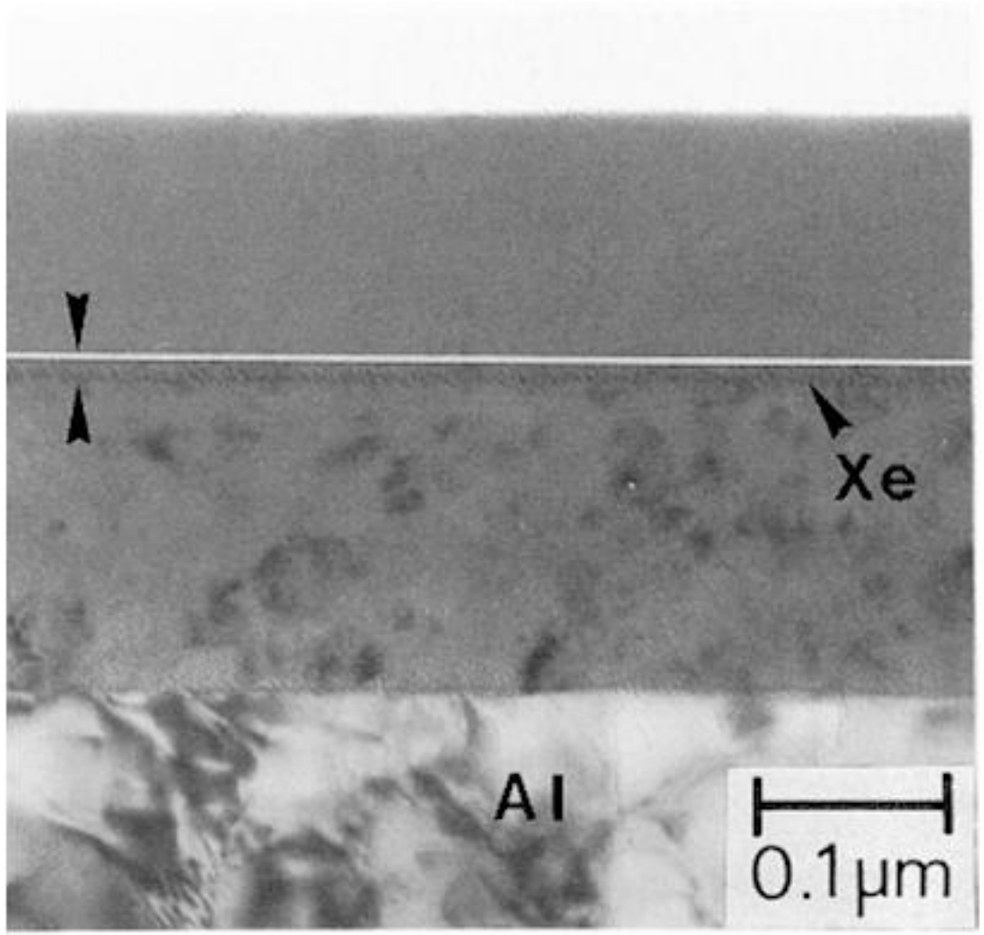

Figure 4

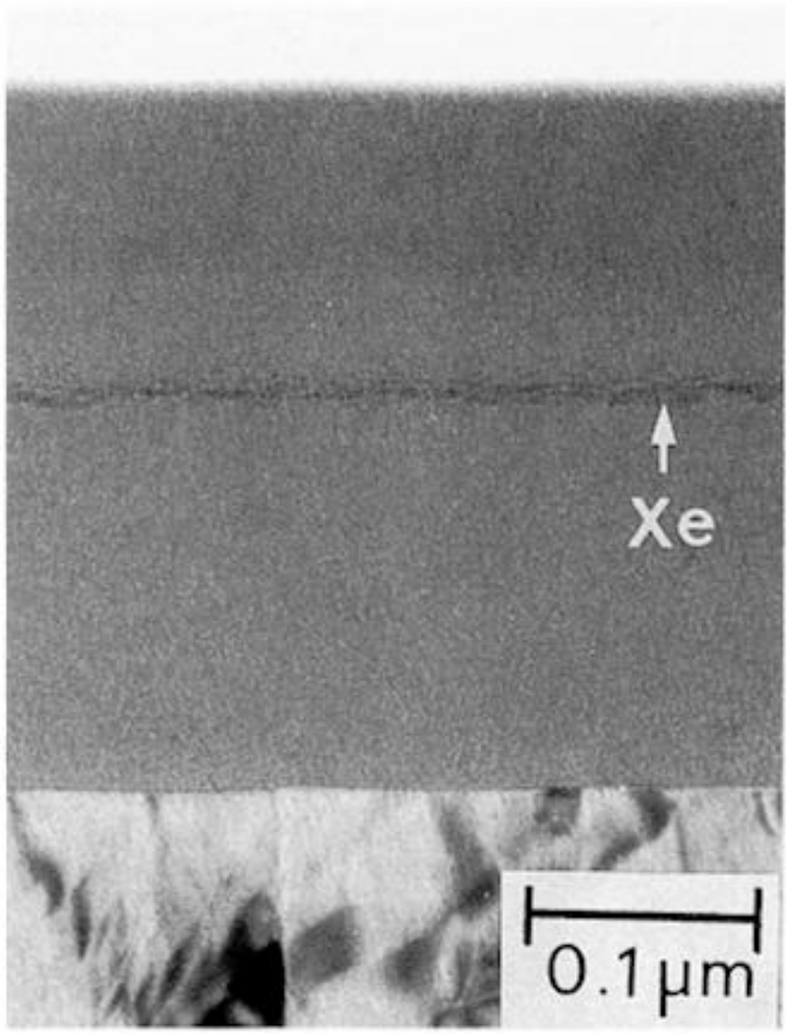

igure 3. As figure 1*a*, but after 10 min exposure in the defocused electron beam of the trans-
ission electron microscope to encourage crystallization.

igure 4. Transmission electron micrograph of an ultramicrotomed section of a barrier oxide film
rmed on aluminium at a constant current density of 5 mA cm^{-2} in 0.1 M sodium tungstate
olution to 250 V at 25 °C, after a thin pre-formed oxide layer was implanted with a xenon
arker layer.

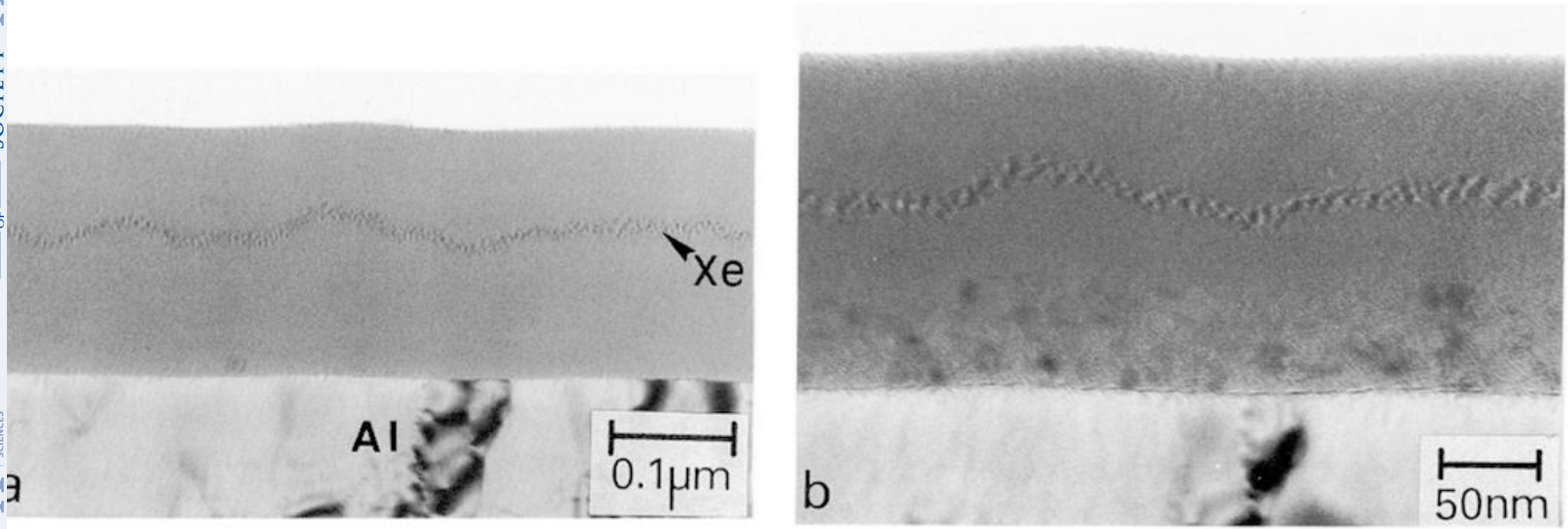

Figure 5. (*a*) Transmission electron micrograph of ultramicrotomed section of the barrier oxide film formed on aluminium at a constant current density of 5 mA cm^{-2} in 0.1 M ammonium dihydrogen phosphate solution to 180 V at 25 °C, after a thin preformed oxide layer was implanted with a xenon marker layer. (*b*) As (*a*), but after 10 min exposure with a defocused electron beam to encourage crystallization.

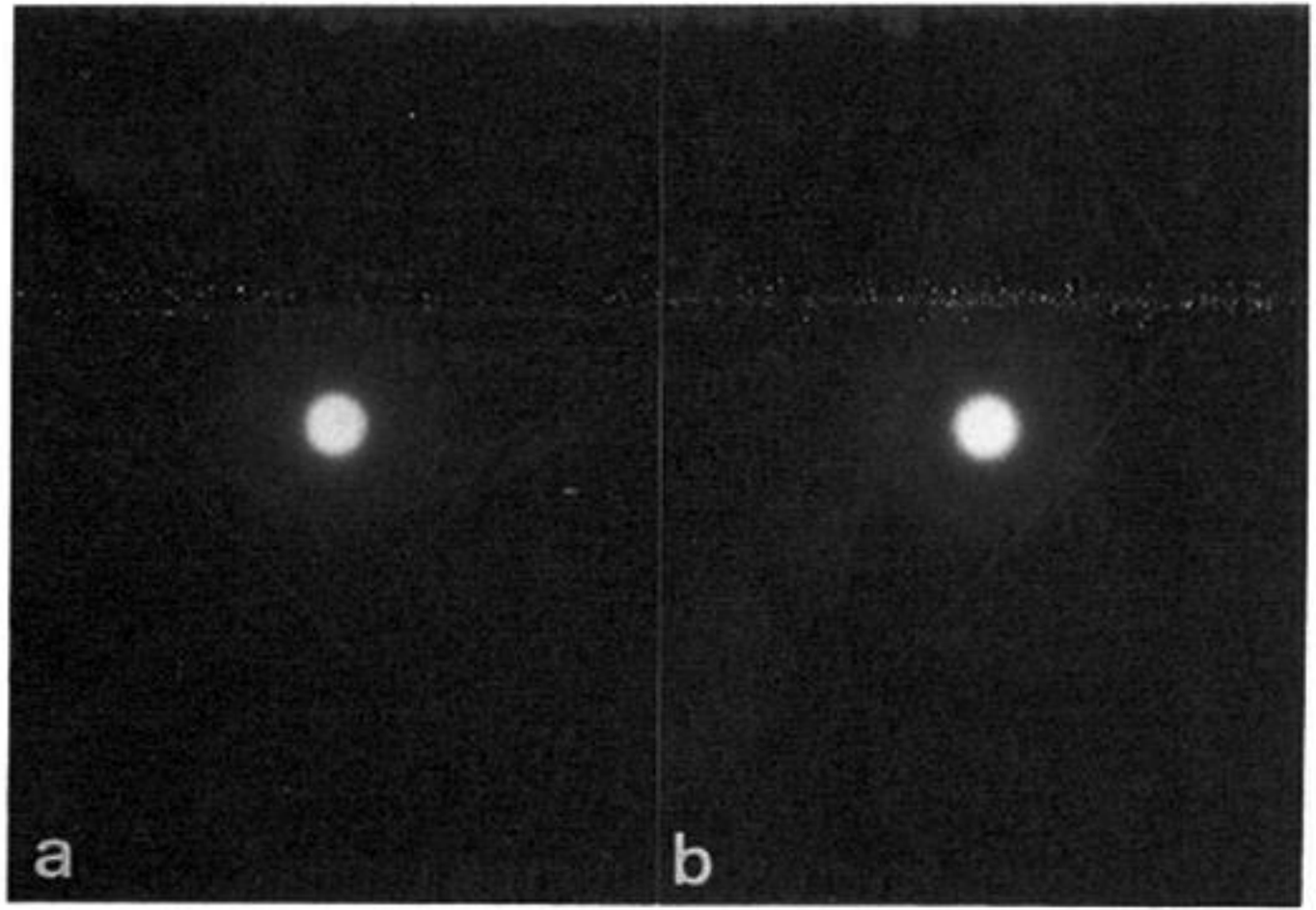

Figure 6. Microdiffraction patterns obtained from the inner, pure oxide layer of anodic alumina. (*a*) Before annealing. (*b*) After annealing at 450 °C for 1 h.

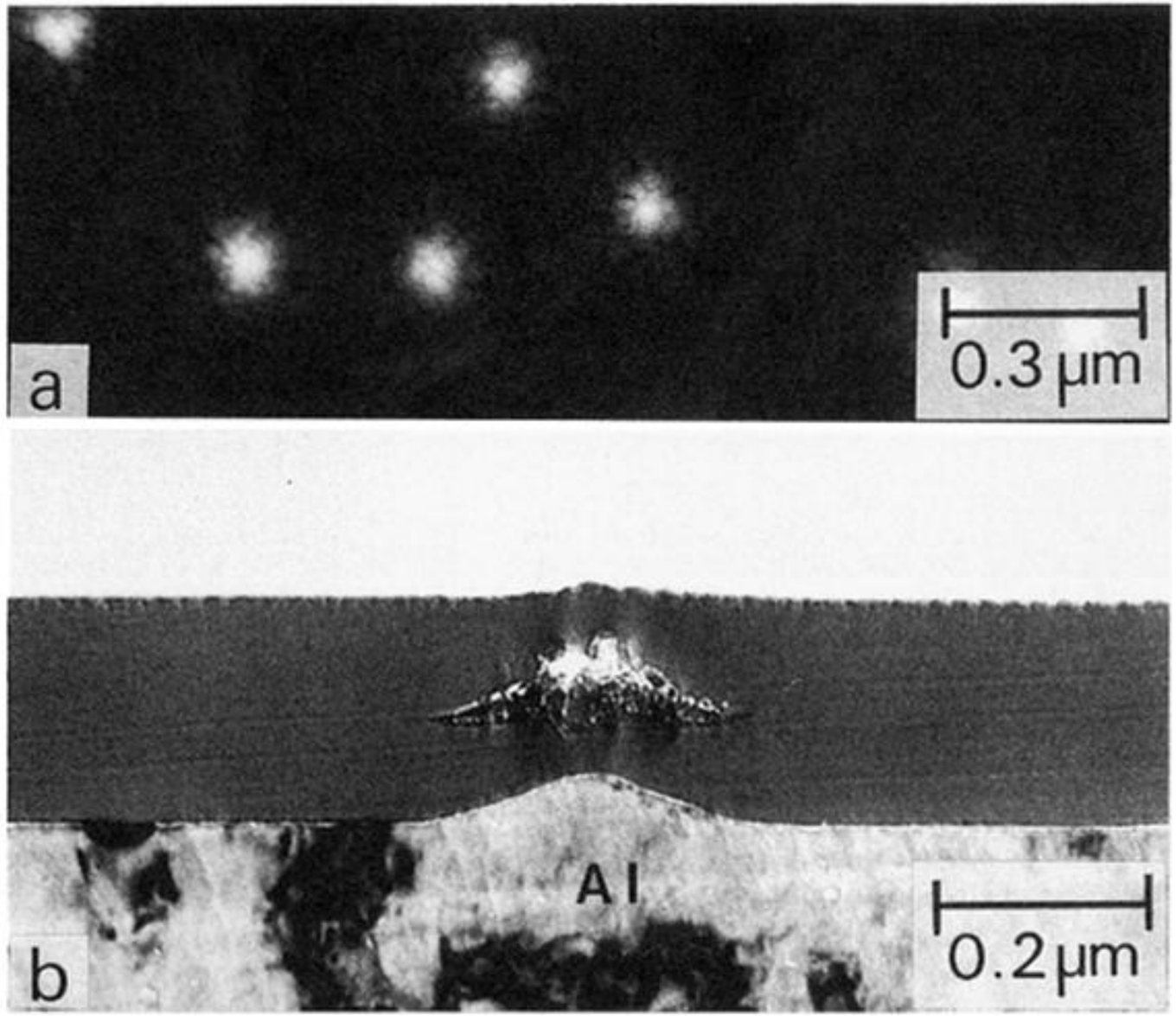

Figure 7. γ'-alumina crystals in a barrier oxide film formed on aluminium covered with a thin thermal oxide layer. (*a*) Stripped oxide film. (*b*) Cross-section. In the stripped film, γ'-alumina crystals appear as lighter, finely textured regions, about 300 nm in diameter. Here, an electropolished aluminium specimen was heated in air at 500 °C for 10 min and, subsequently, anodized at a constant current density of 5 mA cm^{-2} in 0.1 M ammonium pentaborate solution to 175 V.

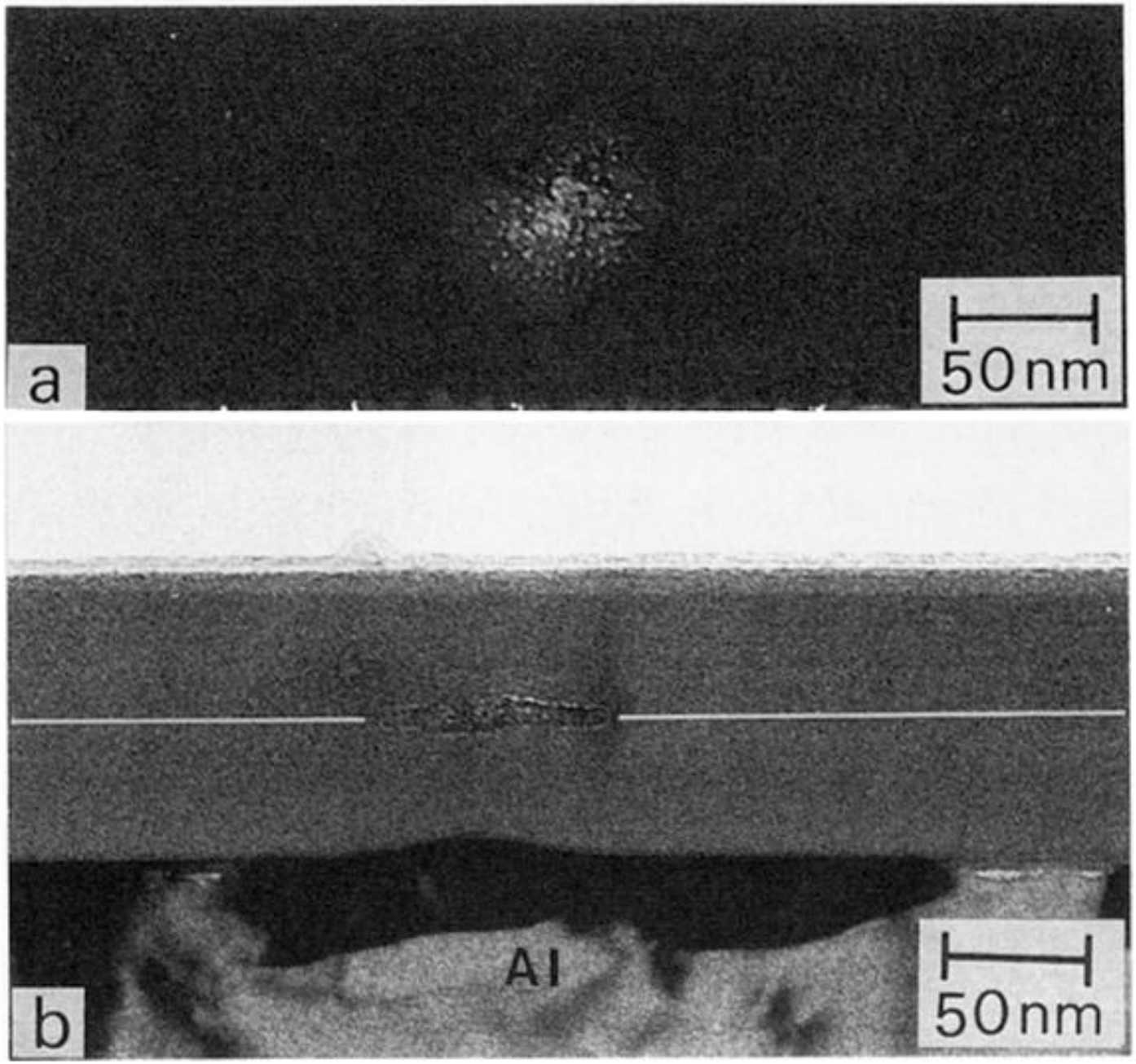

igure 9. As figure 7, but formed to 100 V in order to determine the transport numbers from the location of the γ-alumina crystals.

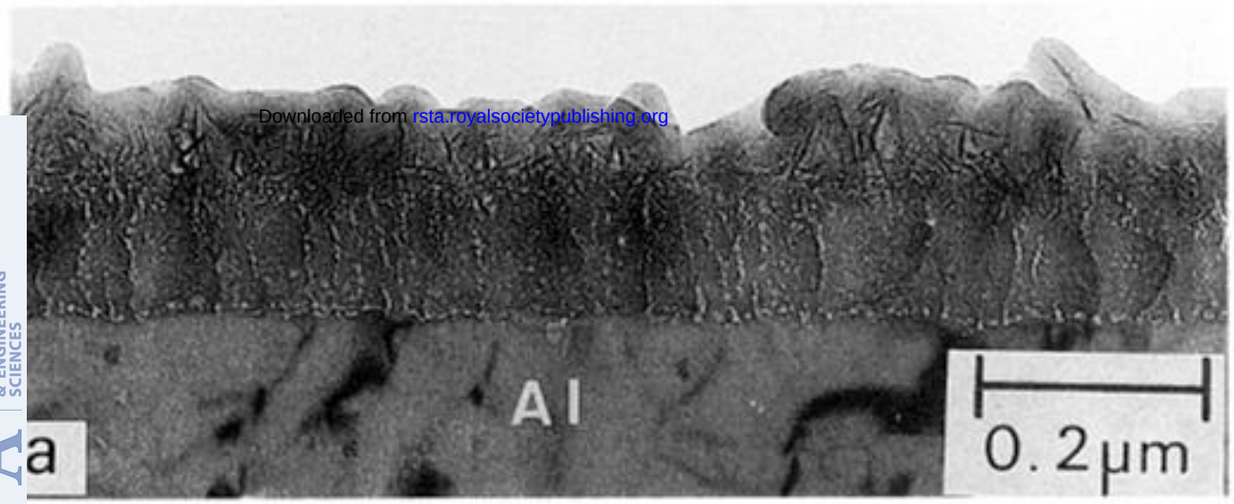

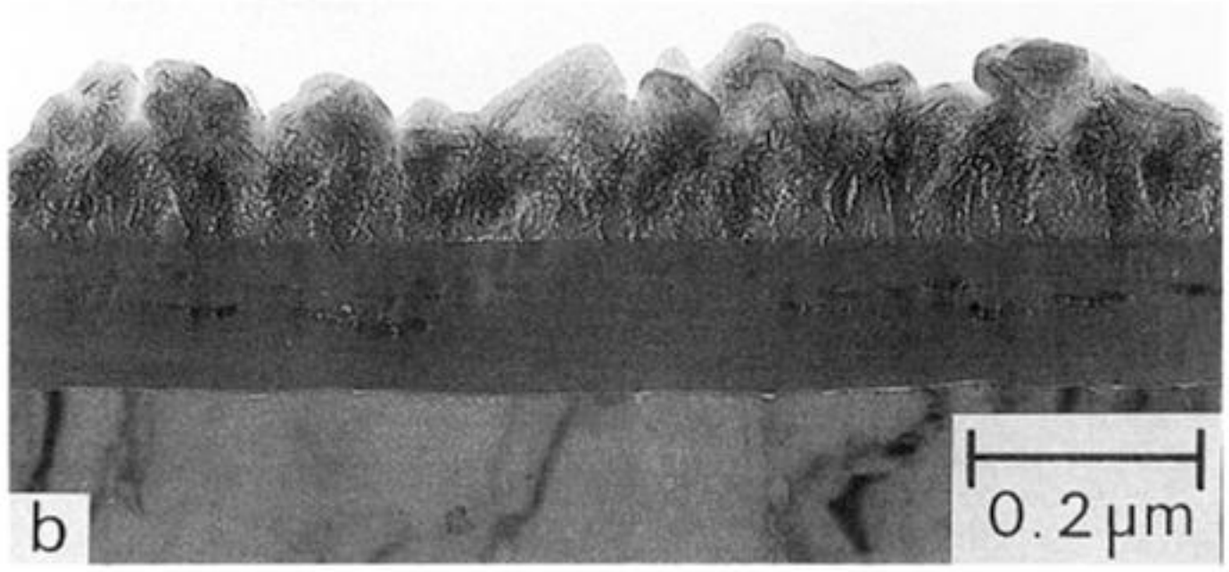

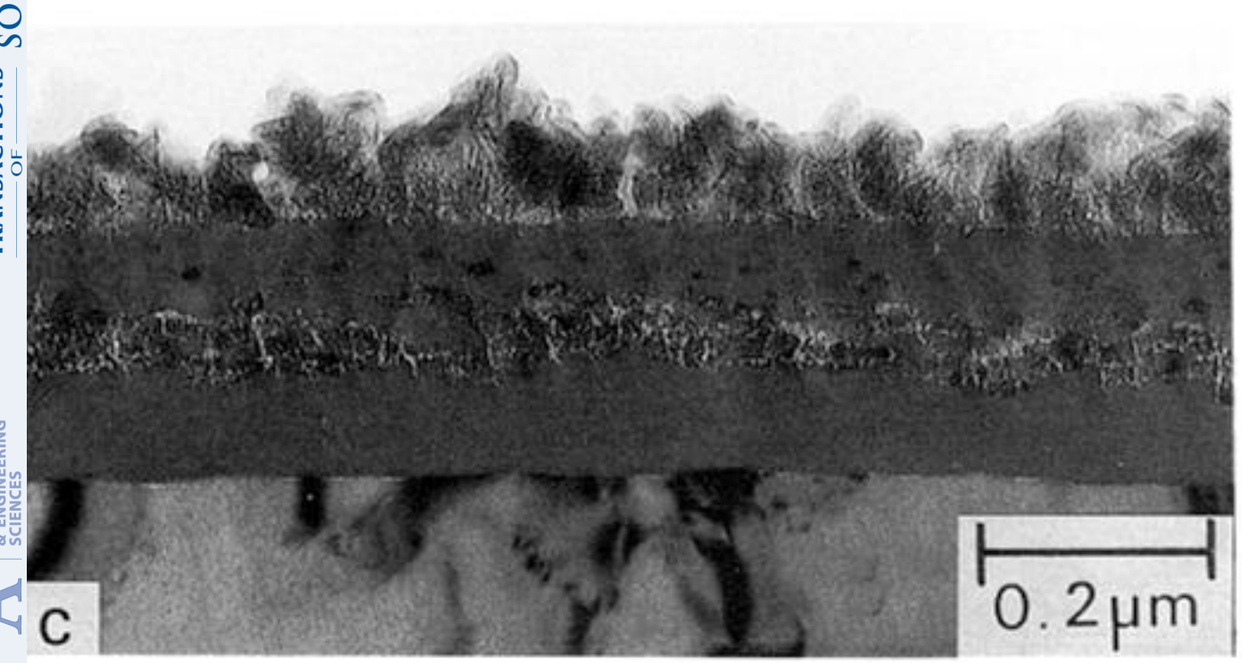

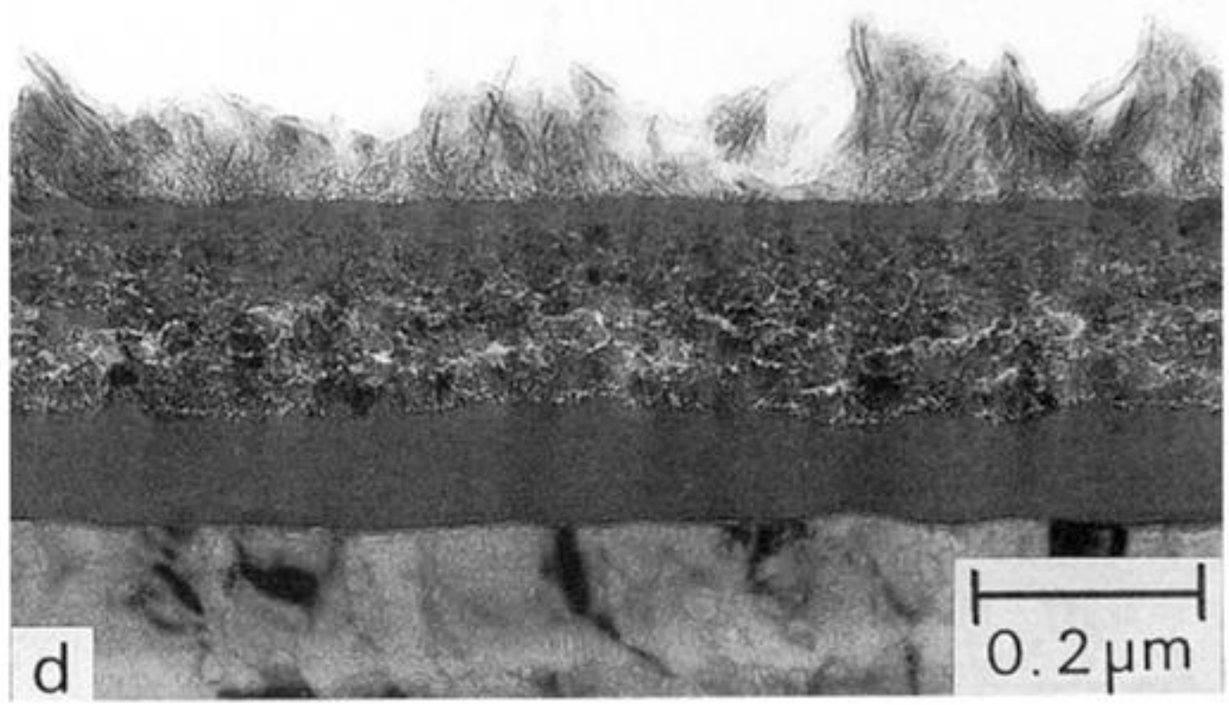

Figure 10. Transmission electron micrographs of ultramicrotomed sections of hydrous oxide film and composite barrier oxide films. (*a*) Hydrous oxide layer formed on electropolished aluminium specimens which were immersed in boiling distilled water for 5 min. (*b*) As in (*a*) after being anodized at a constant current density of 5 mA cm^{-2} in 0.1 M ammonium pentaborate solution to 100 V at 25 °C. (*c*) As in (*a*) and then anodized to 200 V. (*d*) As in (*a*) and then anodized to 300 V.

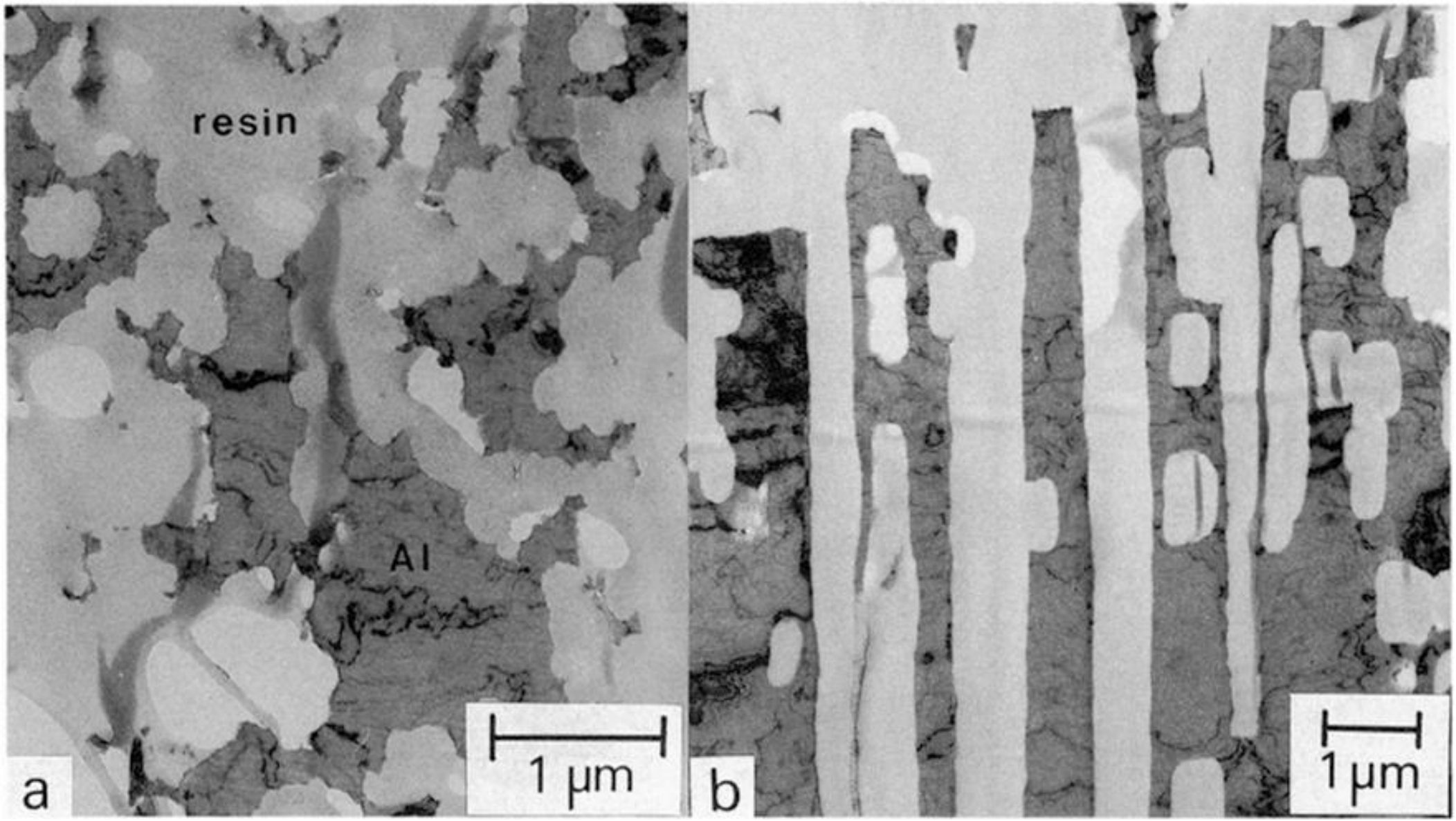

Figure 12. Transmission electron micrographs of ultramicrotomed sections of etched aluminium foils for capacitor applications. (*a*) An aluminium foil etched under AC conditions. (*b*) An aluminium foil etched by DC.

PHILOSOPHICAL TRANSACTIONS OF THE ROYAL SOCIETY A MATHEMATICAL, PHYSICAL & ENGINEERING SCIENCES

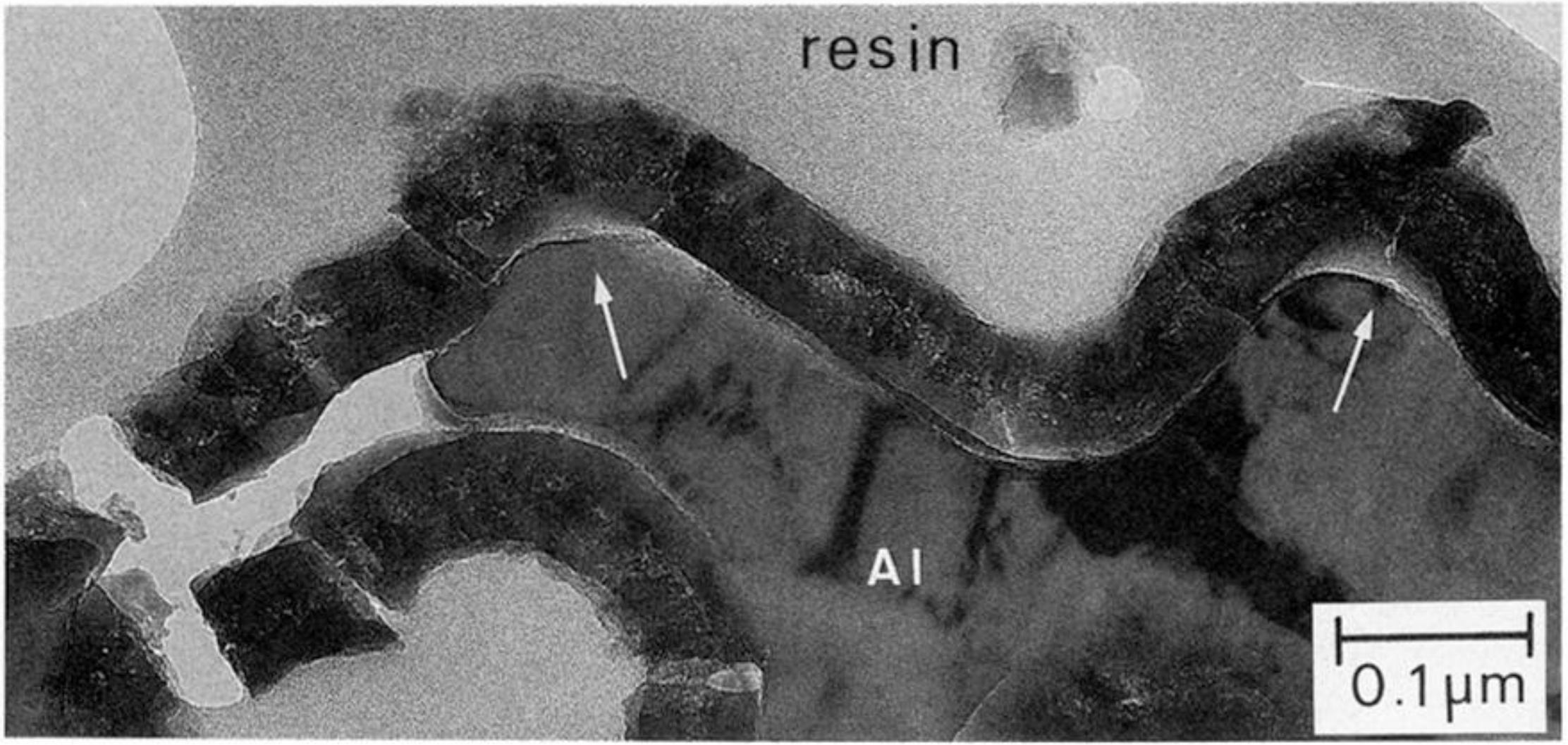

igure 13. Transmission electron micrograph of an ultramicrotomed section of the barrier oxide film, formed on an AC etched aluminium foil.

igure 14. Transmission electron micrograph on an ultramicrotomed section of the porous oxide lm grown in an Al–1.5 wt% Fe alloy at a constant current density of 5 mA cm^{-2} in 2.4 M ulphuric acid at 25 °C for 2 min.

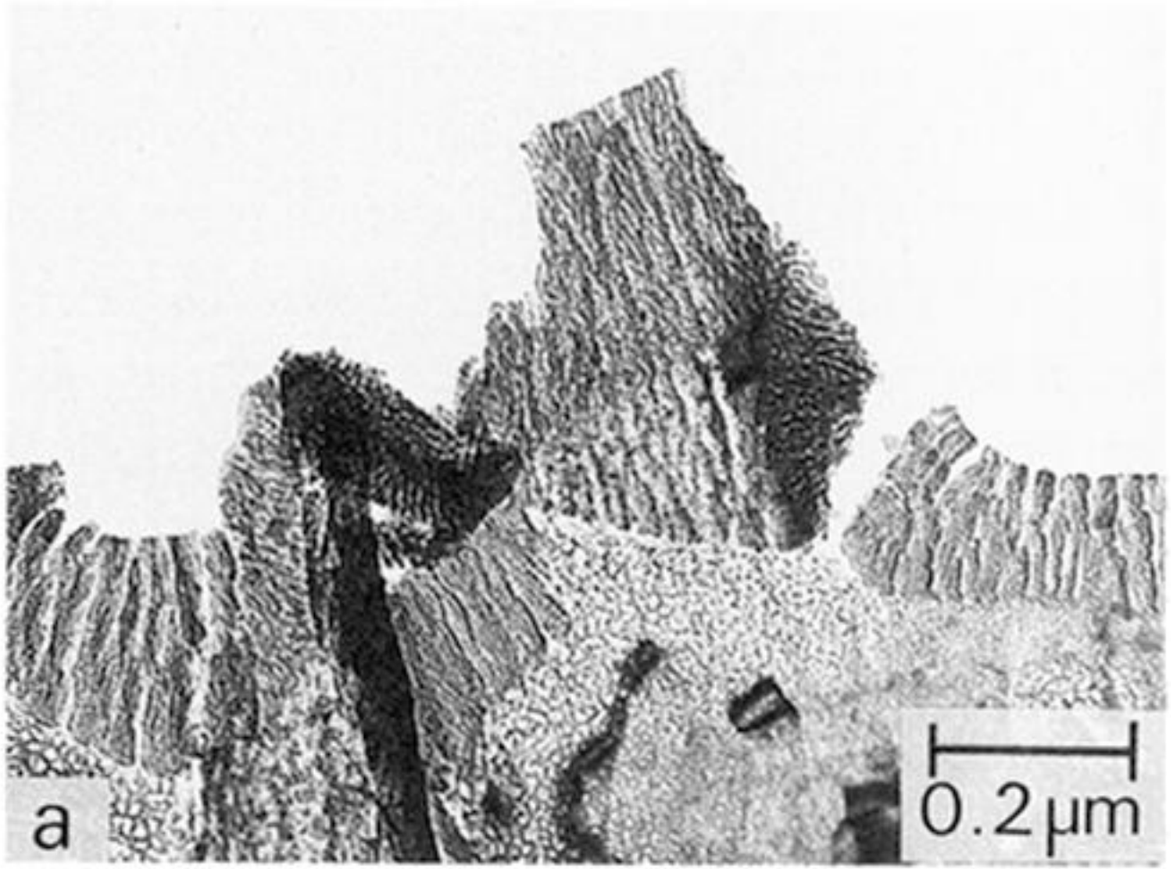

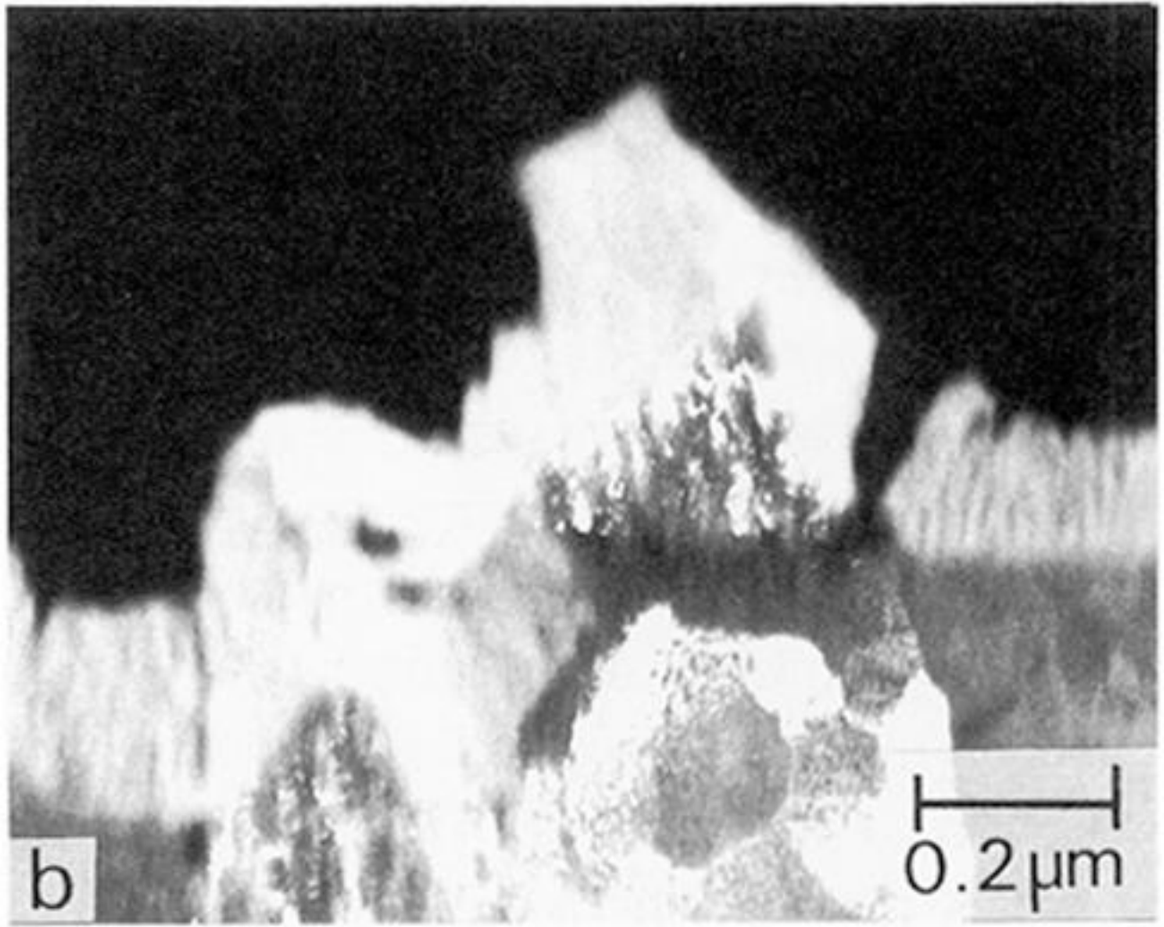

igure 15. Enlargement of a local area in figure 14. (*a*) Bright field micrograph. (*b*) Micrograph revealed by crudely displacing the objective aperture from the transmitted beam location.

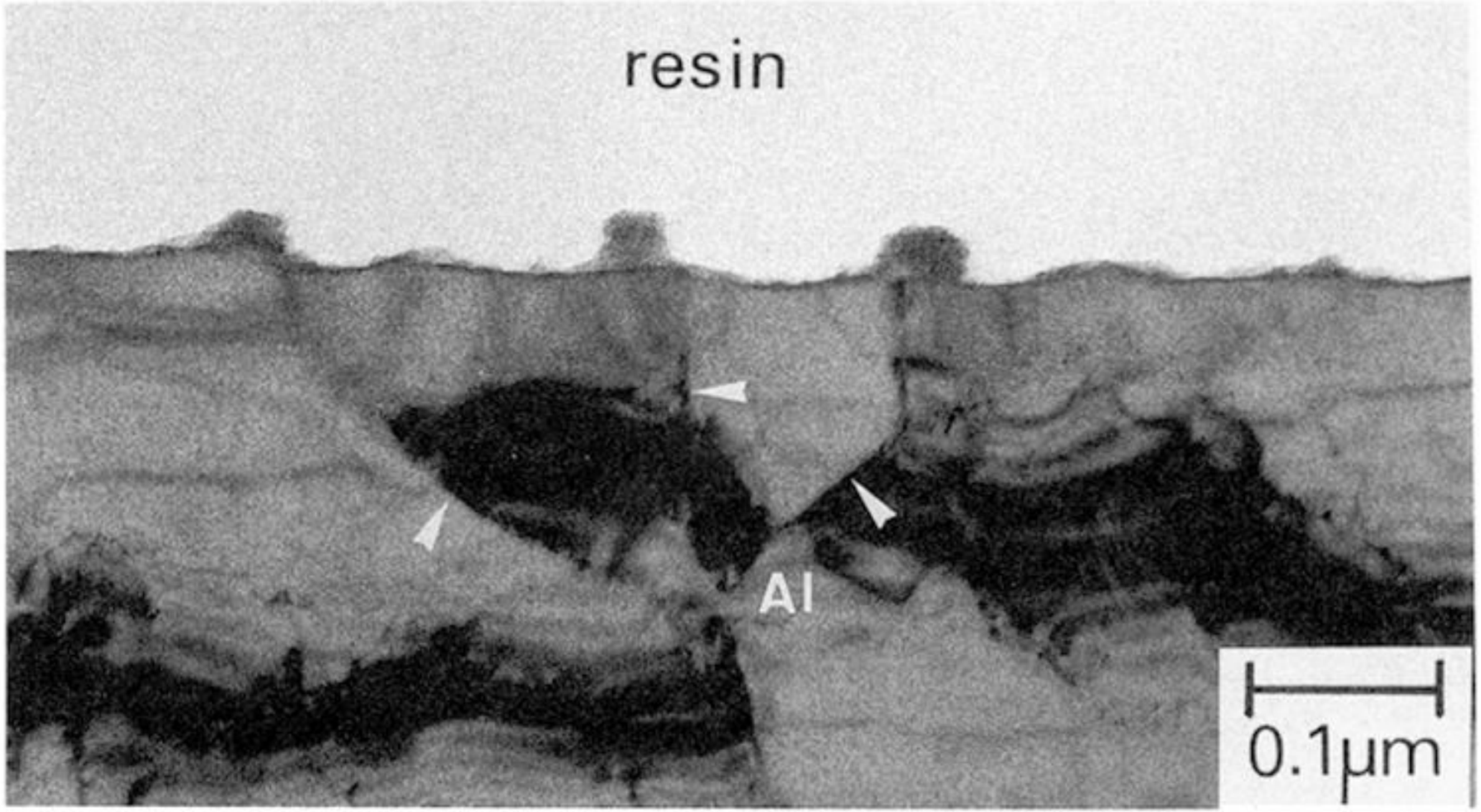

Figure 16. Transmission electron micrograph of an ultramicrotomed section of an electropolished, high purity, aluminium specimen which was immersed for 5 s in an acid chromate chemical conversion coating bath.

Figure 17

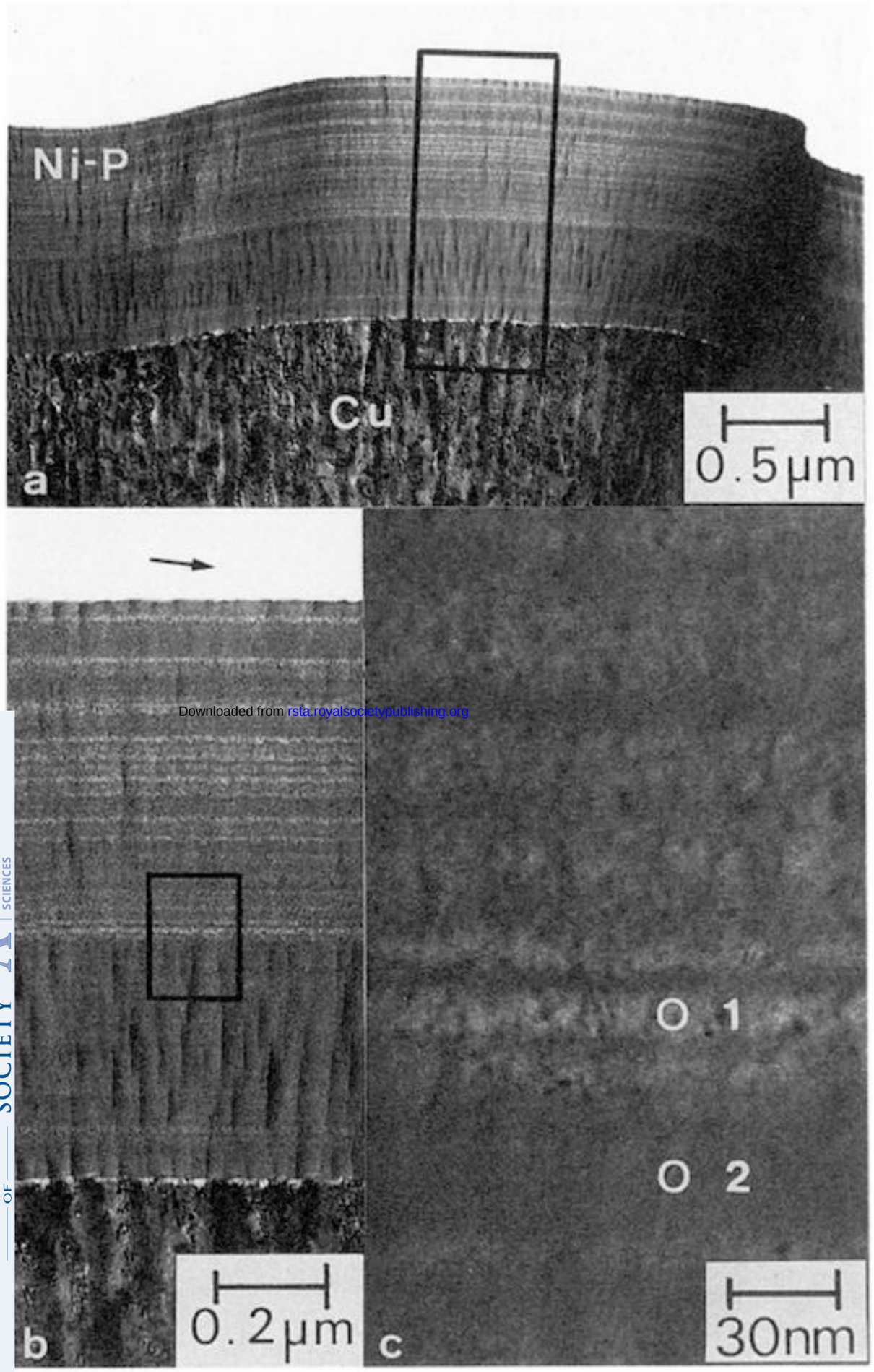

Figure 18

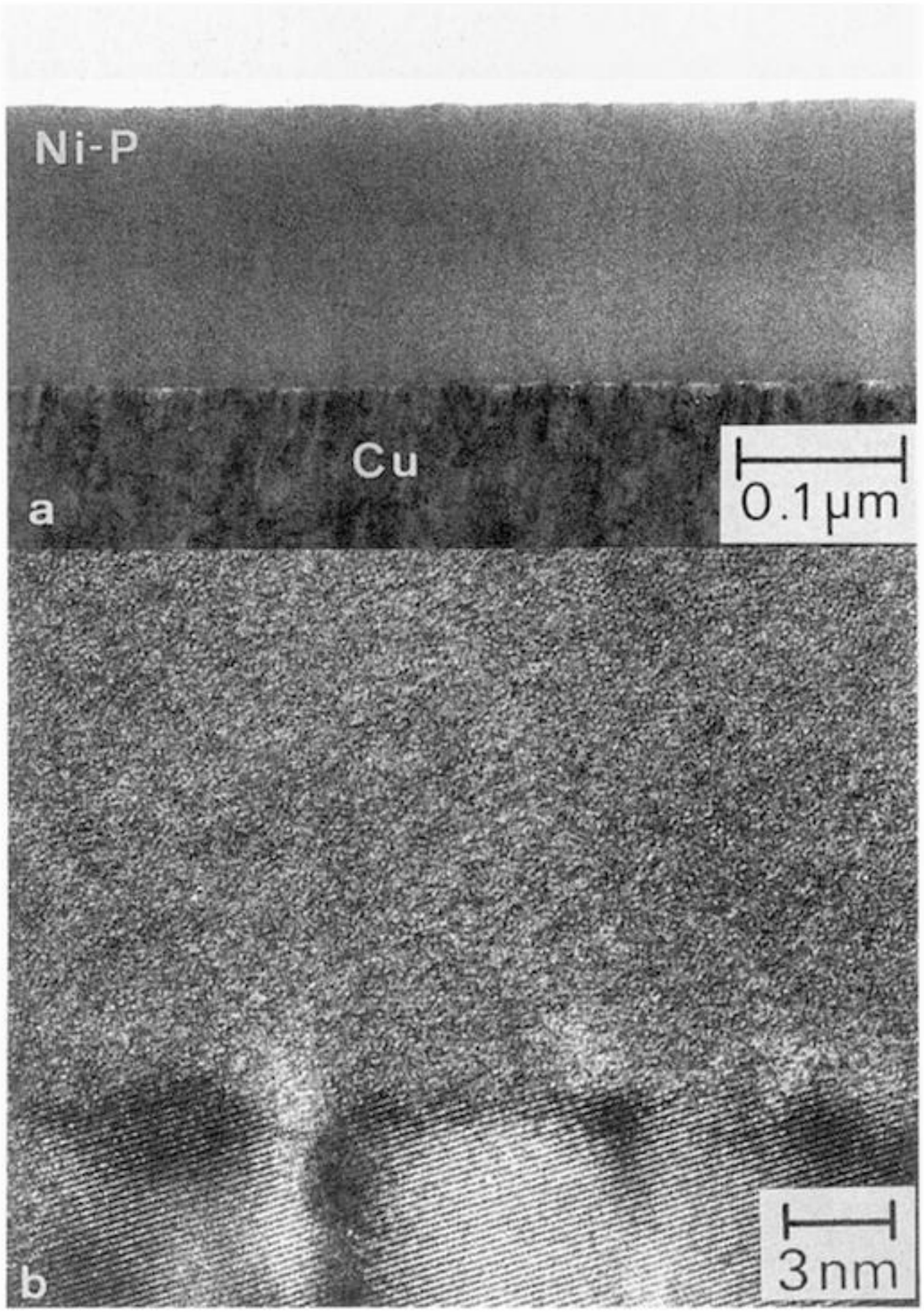

Figure 17. Transmission electron micrograph of an ultramicrotomed section of Ni_{86}–P_{14} alloy, showing the presence of fine layers of different crystallinity. The alloy was electrodeposited from a nickel sulphate, nickel chloride, boric acid and phosphoric acid mixture, using a current density of 5 A dm^{-2} at 70 °C for 1 min. (*a*) General view. (*b*) An enlargement of the boxed area shown in (*a*). (*c*) An enlargement of the boxed area shown in (*b*). EDX analysis of local areas shown in (*c*) indicates that the phosphorus content in probe position (1) is less than in probe position (2).

Figure 18. Transmission electron micrograph of an ultramicrotomed section of Ni_{77}–P_{23} alloy. (*a*) General view. (*b*) High resolution image, showing the presence of an 'ordered region', a few nanometres in size, in the alloy.

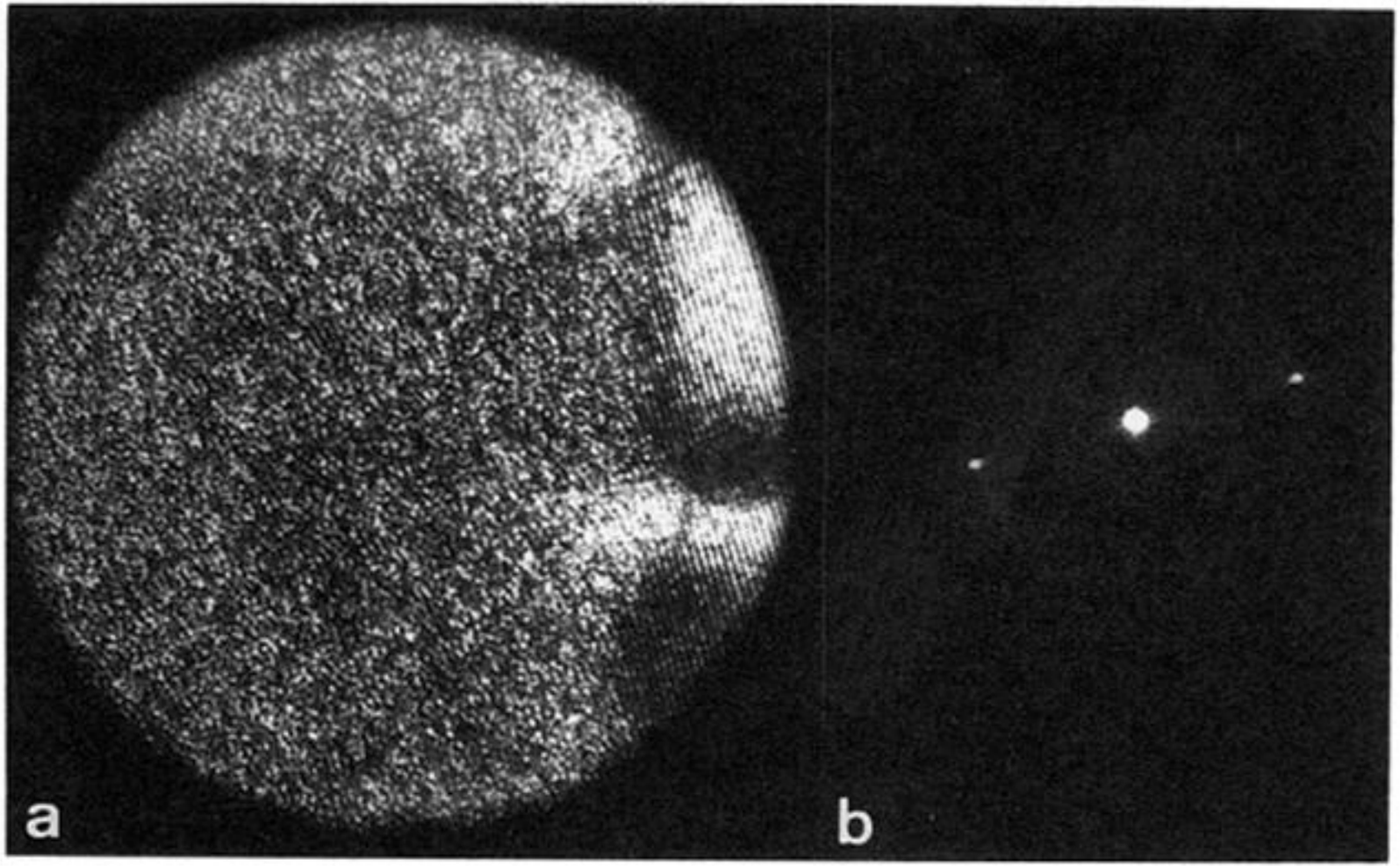

igure 19. (a) Local area in figure 18b. (b) Fourier transform obtained from the local area shown in (a).

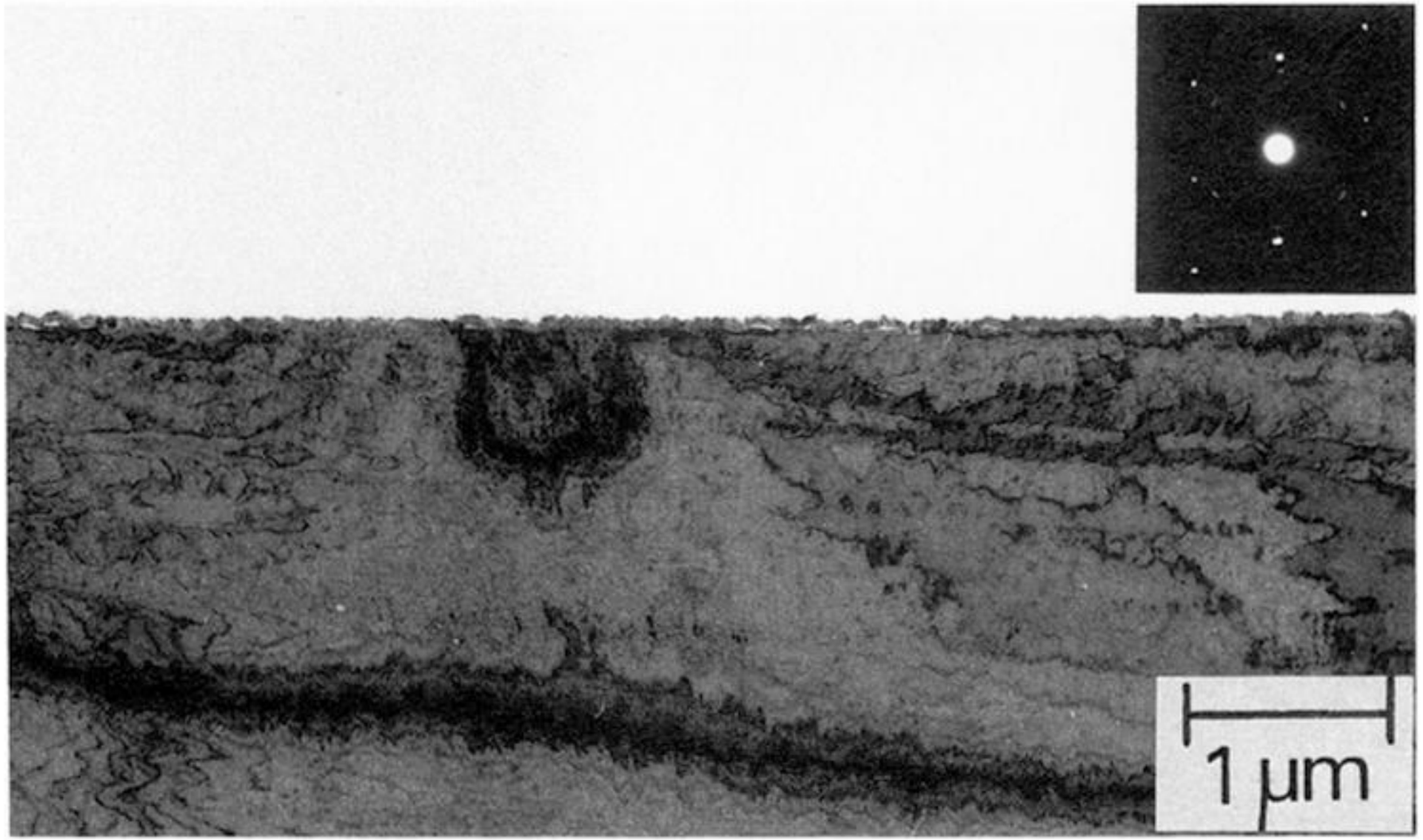

igure 20. Transmission electron micrograph of an ultramicrotomed section of the thermal oxide lm grown on the (111) face of copper which has been oxidized in purified oxygen at 178 °C for 0 min.

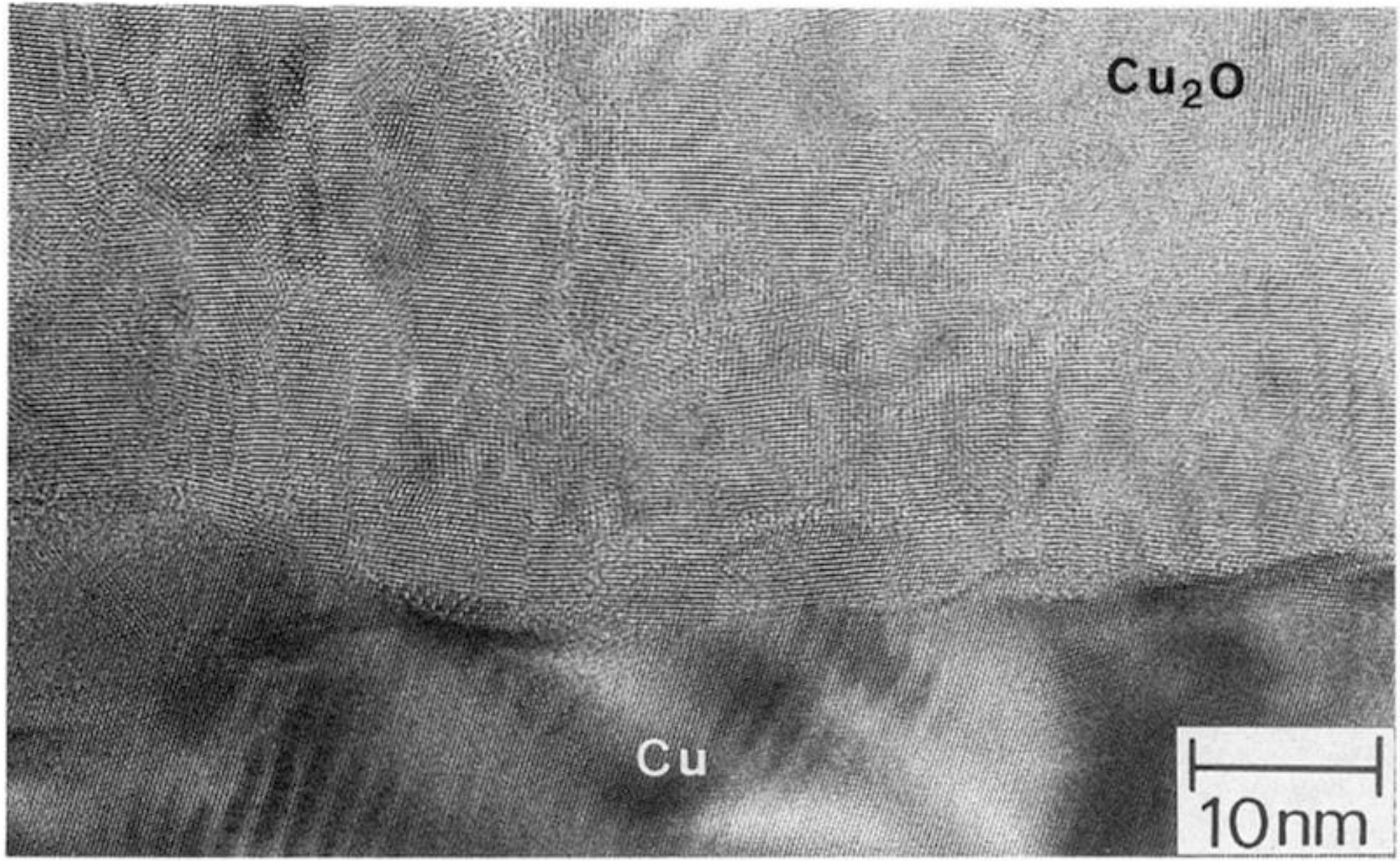

igure 21. High resolution image of the copper–oxide interface, revealing the epitaxial interaction etween the metal and oxide and consequent development of the mosaic structure in the oxide.

PHILOSOPHICAL TRANSACTIONS OF THE ROYAL SOCIETY A MATHEMATICAL, PHYSICAL & ENGINEERING SCIENCES